SESSION IX

FUEL FABRICATION AND REPROCESSING

Wednesday, August 30, 1972
CHAIRMAN: F. D. Fisher

CHAIRMAN'S OPENING REMARKS:

Unfortunately, from my selfish point of view, it appears from the titles and the preprints that I am the only pellet presser up here, i.e., fuel fabricator. This session will deal exclusively with reprocessing. It appears that we are to be treated to a real pot-pourri of reprocessing-related subjects. Appropriately enough, we will begin with head-end processing and we will wind up with waste management.

AN ESTIMATE OF THE PROCESS DECONTAMINATION FACTORS REQUIRED TO MEET FEDERAL EFFLUENT REGULATIONS FOR THE BURNING OF HTGR FUEL ELEMENTS*

J.W. Snider and R.E. Leuze
Oak Ridge National Laboratory
Oak Ridge, Tennessee

Abstract

Calculations are made of the various quantities of air required (theoretically) to dilute 139 isotopes, present at two reprocessing times, in HTGR fuel elements to meet existing federal effluent regulations. One isotope (Pu-238) represents 79% of the total, calculated isotopic potential hazard from the burning of HTGR fuel elements. The largest calculated decontamination factor required was 640,000 for Pu-238.

I. Introduction

The design philosophy of a plant for reprocessing the fueled graphite from a high-temperature gas-cooled reactor (HTGR) will be influenced by the existing regulations with regard to gaseous and liquid effluents. These regulations affect the inclusion or omission of certain process steps, gaseous and liquid waste handling procedures, structural integrities, equipment arrangements, etc. A useful way for the process designer to use the effluent regulations is to express them as overall process decontamination factors for the various amounts of isotopes actually present in the spent fuel elements at reprocessing time.

The proposed method for reprocessing HTGR fuel consists, in part, of burning the graphite fuel elements in air or oxygen and separating the fissile and fertile materials from the fission products by solvent extraction methods. The first step in this process is unprecedented in nuclear fuel reprocessing in that the fuel elements are prepared for dissolution by combustion. The large quantity of carbon present in the fuel elements is converted into carbon dioxide during this combustion step. This carbon dioxide, being formed in intimate contact with the spent fuel, will be contaminated with fission products.

At present it is not possible to predict the quantities of all of the isotopes or their chemical or physical forms in the carbon dioxide. However, some comparative means of estimating the decontamination factors actually required for the various amounts of the isotopes present would be useful in identifying the isotopes which will require the most attention during actual processing.

The isotopes that are of the most concern in HTGR reprocessing plant liquid effluents are those the reprocessing industry is presently aware of because of the similarity of these effluents to Light Water Reactor liquid wastes. This is not true for the gaseous effluents. The isotopes that will be present as contaminants in the carbon dioxide must first be identified and the appropriate off-gas decontamination processes developed. The identities of those that will

*Research sponsored by the U.S. Atomic Energy Commission under contract with the Union Carbide Corporation.

be present as contaminants in the carbon dioxide must await hot-cell combustion studies using irradiated fuels. This paper presents an estimate of the overall gaseous process decontamination factors for 139 isotopes present in HTGR fuels at reprocessing times of 150 and 365 days after irradiation. The calculational model assumes that the fuel is completely vaporized during the burning process and calculates the overall gaseous process decontamination factors for this vapor. It should be noted that the burning process itself gives high gaseous decontamination factors for the nonvolatile isotopes.

II. Estimation of the Significant Isotopes Present at Reprocessing Time

An estimate of the quantities of the various isotopes present in six-year-irradiated Fort St. Vrain Reactor fuel at reprocessing time was made using the ORIGEN isotope generation and decay code[1]. The ORIGEN library contains nuclear transmutations by n-γ, n-α, n-p, n-2n, n-3n, and n-fission products plus radioactive decay by β^-, β^+, and alpha decay and isomeric transitions. The ORIGEN code computes the isotope inventories of more than 700 isotopes in the fuel as a function of the length of irradiation and postirradiation time. The elements whose isotopes are included in the ORIGEN library are shown in Figure 1.

The following conditions were assumed for calculational purposes:

1. The fuel elements are of the Fort St. Vrain[2] HTGR type shown in Figure 2.

2. The fissile material is ^{235}U, and the fertile material is ^{232}Th homogeneously mixed with the carbon.

3. The carbon-to-heavy metal (U+Th) mole ratio is 150.

4. The fuel elements are irradiated for six years at an average flux of 6.63×10^{13} neutrons/sec-cm^2. The burnup is 100,000 MWd per metric ton of initial heavy metal.

5. The graphite block contains 1 ppm of lithium, 162 ppm of boron, 100 ppm of nitrogen, 17 ppm of silicon, and 50 ppm of iron as contaminants.

The results of the ORIGEN calculations are shown in Table 1 for 150- and 365-day-cooled fuel.

III. Existing Federal Effluent Regulations

Existing regulations for nuclear plant effluents are stated in Title 10, Chapter 1, Code of Federal Regulations, Part 20 (10 CFR, Part 20). The plant effluent concentrations at the plant boundary are specified for the various isotopes in Appendix B, Table II, Column 1, of 10 CFR, Part 20. This regulation limits the annual exposure from plant effluents to individuals living near the plant boundary to not more than 500 millirems per year. Since it is difficult or impossible to predict the exact chemical compounds that could be formed during the burning process, the permissible effluent concentrations used for calculational purposes is the lower of the "soluble" or "insoluble" values of Appendix B, Table II, Column 1 of 10 CFR, Part 20.

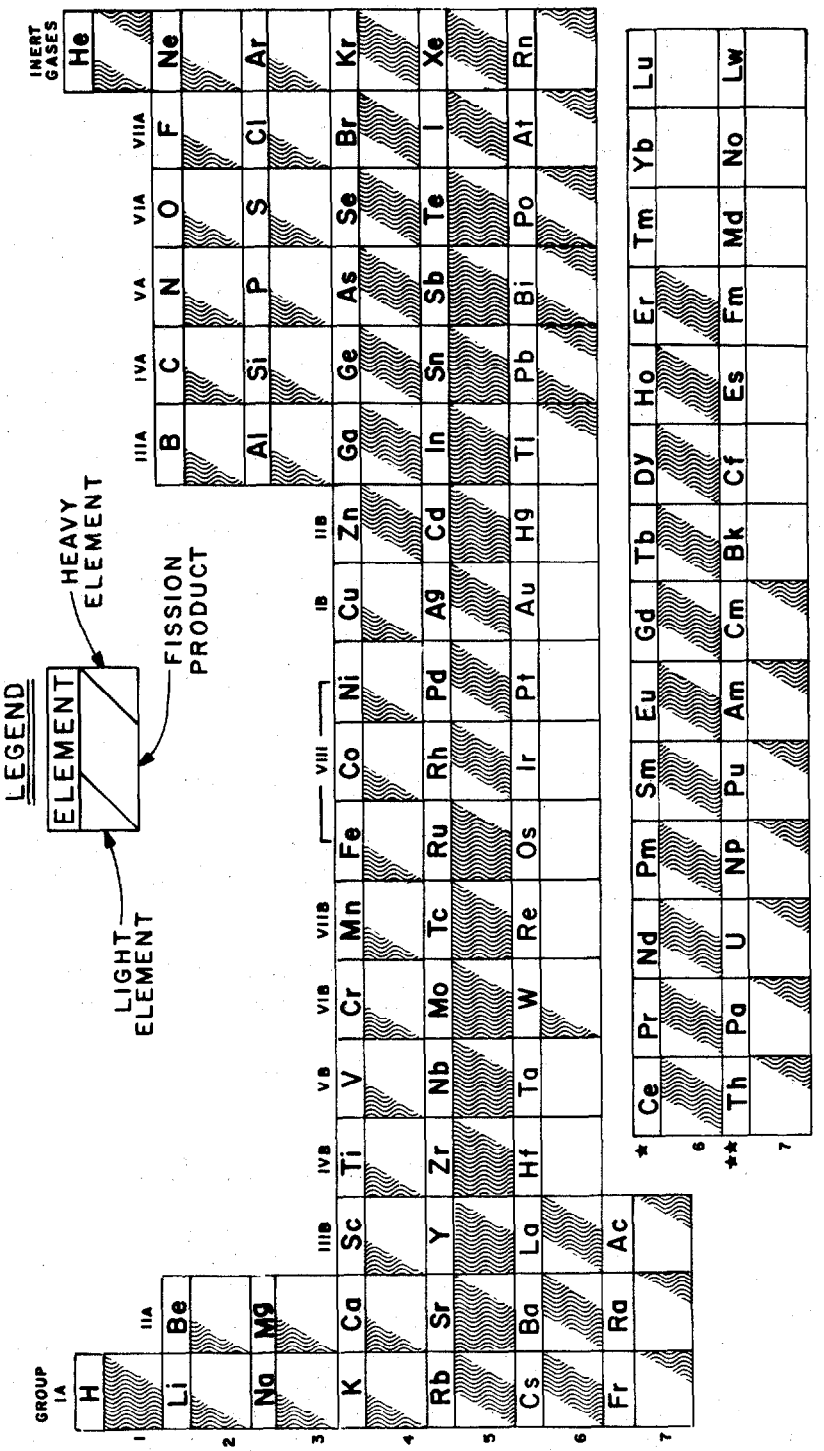

FIGURE 1. ELEMENTS WHOSE ISOTOPES ARE INCLUDED IN THE ORIGEN LIBRARY.

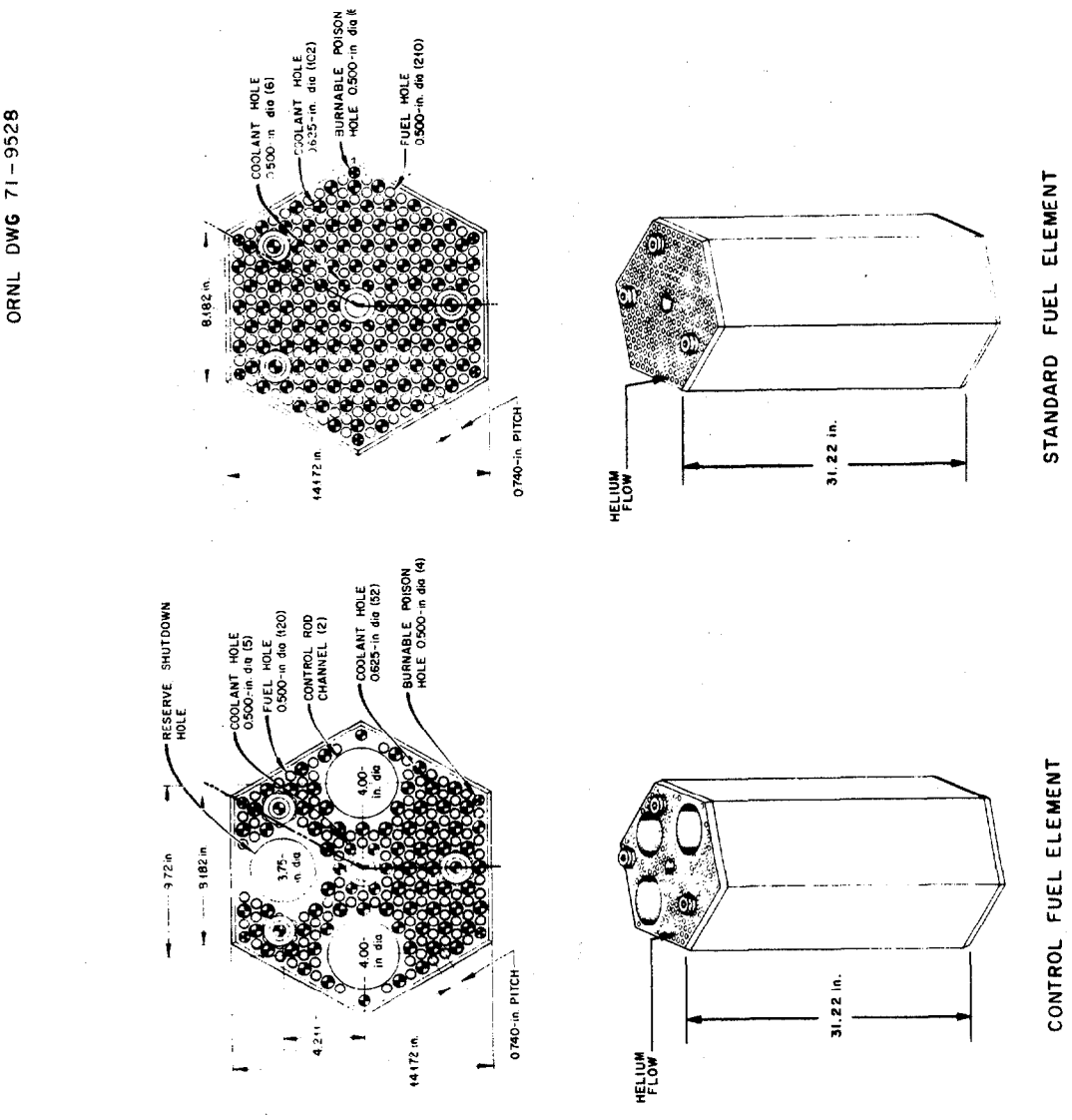

FIGURE 2. SCHEMATIC OF THE FORT ST. VRAIN HTGR REACTOR FUEL ELEMENTS.

Table 1. ORIGEN Calculation of the Radioactive Nuclide Concentrations Present at Reprocessing Time

Isotope	150 Day Cooled (Ci/metric ton)[a]	365 Day Cooled (Ci/metric ton)[a]
^{3}H	4.07×10^{3}	3.94×10^{3}
^{10}Be	1.49×10^{-2}	1.49×10^{-2}
^{14}C	5.91×10^{1}	5.91×10^{1}
^{32}P	1.09×10^{-4}	-
^{51}Cr	1.13×10^{-2}	5.31×10^{-5}
^{54}Mn	9.18×10^{0}	5.61×10^{0}
^{55}Fe	4.99×10^{2}	4.27×10^{2}
^{59}Fe	2.15×10^{0}	7.88×10^{-2}
^{60}Co	2.14×10^{0}	1.98×10^{0}
^{79}Se	2.13×10^{0}	2.13×10^{0}
^{85}Kr	6.56×10^{4}	6.32×10^{4}
^{86}Rb	1.97×10^{1}	6.83×10^{-3}
^{89}Sr	2.39×10^{5}	1.37×10^{4}
^{90}Sr	3.06×10^{5}	3.02×10^{5}
^{90}Y	3.06×10^{5}	3.02×10^{5}
^{91}Y	3.00×10^{5}	2.38×10^{4}
^{93}Zr	7.20×10^{0}	7.20×10^{0}
^{95}Zr	3.83×10^{5}	3.86×10^{4}
^{93m}Nb	1.34×10^{0}	1.52×10^{0}
^{95}Nb	7.17×10^{5}	8.21×10^{4}
^{95m}Nb	8.11×10^{3}	8.20×10^{2}
^{99}Mo	1.04×10^{10}	-
^{99}Tc	3.38×10^{1}	3.38×10^{1}
^{99m}Tc	9.90×10^{-11}	-
^{103}Ru	4.81×10^{4}	1.12×10^{3}
^{106}Ru	8.25×10^{4}	5.50×10^{4}
^{103m}Rh	4.81×10^{4}	1.12×10^{3}
^{106}Rh	8.25×10^{4}	5.50×10^{4}
^{107}Pd	4.78×10^{-2}	4.78×10^{-2}
^{110}Ag	1.55×10^{1}	8.59×10^{0}
^{110m}Ag	1.19×10^{2}	6.61×10^{1}
^{111}Ag	8.81×10^{-3}	2.07×10^{-11}
^{113m}Cd	1.93×10^{-1}	1.87×10^{-1}

Table 1 (Contd.)

Isotope	150 Day Cooled (Ci/metric ton)[a]	365 Day Cooled (Ci/metric ton)[a]
^{115m}Cd	3.73×10^{1}	1.17×10^{0}
^{117m}Sm	1.57×10^{-4}	-
^{119m}Sn	9.24×10^{0}	5.09×10^{0}
^{123m}Sn	6.41×10^{2}	1.95×10^{2}
^{125}Sn	2.39×10^{-1}	-
^{126}Sn	1.22×10^{0}	1.22×10^{0}
^{124}Sb	3.05×10^{2}	2.55×10^{1}
^{125}Sb	1.92×10^{4}	1.65×10^{4}
^{126}Sb	8.10×10^{0}	1.21×10^{0}
^{126m}Sb	1.22×10^{0}	1.22×10^{0}
^{127}Sb	3.84×10^{-7}	-
^{123m}Te	3.00×10^{0}	8.39×10^{-1}
^{125m}Te	7.84×10^{3}	6.84×10^{3}
^{127}Te	1.50×10^{4}	3.82×10^{3}
^{127m}Te	1.52×10^{4}	3.87×10^{3}
^{129}Te	6.37×10^{3}	7.94×10^{1}
^{129m}Te	9.93×10^{3}	1.24×10^{2}
^{132}Te	1.70×10^{-8}	-
^{129}I	1.34×10^{-1}	1.34×10^{-1}
^{131}I	2.27×10^{0}	2.07×10^{-8}
^{132}I	1.75×10^{-8}	-
^{129m}Xe	7.04×10^{-4}	-
^{131m}Xe	3.42×10^{0}	1.13×10^{-5}
^{133}Xe	6.00×10^{-3}	-
^{134}Cs	7.49×10^{5}	6.14×10^{5}
^{135}Cs	9.29×10^{-1}	9.29×10^{-1}
^{136}Cs	6.53×10^{1}	-
^{137}Cs	3.25×10^{5}	3.20×10^{5}
^{137m}Ba	3.04×10^{5}	2.99×10^{5}
^{140}Ba	4.99×10^{2}	4.39×10^{-3}
^{140}La	5.74×10^{2}	5.05×10^{-3}
^{141}Ce	8.82×10^{4}	8.87×10^{2}
^{144}Ce	1.04×10^{6}	6.14×10^{5}

Table 1 (Contd.)

Isotope	150 Day Cooled (Ci/metric ton)[a]	365 Day Cooled (Ci/metric ton)[a]
^{143}Pr	1.03×10^{3}	1.95×10^{-2}
^{144}Pr	1.04×10^{6}	6.14×10^{5}
^{147}Nd	6.89×10^{1}	1.02×10^{-4}
^{147}Pm	1.18×10^{5}	1.01×10^{5}
^{148}Pm	4.62×10^{1}	1.33×10^{0}
^{148m}Pm	5.75×10^{2}	1.66×10^{1}
^{151}Sm	5.68×10^{2}	5.66×10^{2}
^{152m}Eu	3.57×10^{0}	3.45×10^{0}
^{152}Eu	3.57×10^{0}	3.45×10^{0}
^{154}Eu	1.27×10^{4}	1.24×10^{4}
^{155}Eu	1.07×10^{4}	8.52×10^{3}
^{156}Eu	5.79×10^{2}	2.80×10^{-2}
^{162}Gd	1.65×10^{1}	1.10×10^{1}
^{160}Tb	2.35×10^{2}	2.97×10^{1}
^{161}Tb	1.39×10^{-5}	-
^{162m}Tb	1.65×10^{1}	1.10×10^{1}
^{207}Tl	9.29×10^{-2}	1.04×10^{-1}
^{208}Tl	4.78×10^{1}	5.44×10^{1}
^{209}Tl	1.62×10^{-3}	1.80×10^{-3}
^{209}Pb	9.13×10^{-2}	1.01×10^{-1}
^{211}Pb	9.33×10^{-2}	1.04×10^{-1}
^{212}Pb	1.33×10^{2}	1.51×10^{2}
^{211}Bi	9.33×10^{-2}	1.04×10^{-1}
^{212}Bi	1.33×10^{2}	1.51×10^{2}
^{213}Bi	9.13×10^{-2}	1.01×10^{-1}
^{212}Po	8.50×10^{1}	9.66×10^{1}
^{213}Po	8.93×10^{-2}	9.93×10^{-2}
^{215}Po	9.33×10^{-2}	1.04×10^{-1}
^{216}Po	1.33×10^{2}	1.51×10^{2}
^{217}At	9.13×10^{-2}	1.01×10^{-1}
^{219}Rn	9.33×10^{-2}	1.04×10^{-1}
^{220}Rn	1.33×10^{2}	1.51×10^{2}
^{221}Fr	9.13×10^{-2}	1.01×10^{-1}
^{223}Fr	1.07×10^{-3}	1.18×10^{-3}

Table 1 (Contd.)

Isotope	150 Day Cooled (Ci/metric ton)[a]	365 Day Cooled (Ci/metric ton)[a]
^{223}Ra	9.33×10^{-2}	1.04×10^{-1}
^{224}Ra	1.33×10^{2}	1.51×10^{2}
^{226}Ra	9.19×10^{-2}	1.01×10^{-1}
^{228}Ra	5.52×10^{-2}	5.74×10^{-2}
^{225}Ac	9.13×10^{-2}	1.01×10^{-1}
^{227}Ac	9.52×10^{-2}	1.05×10^{-1}
^{228}Ac	5.52×10^{-2}	5.75×10^{-2}
^{227}Th	9.27×10^{-2}	1.02×10^{-1}
^{228}Th	1.33×10^{2}	1.50×10^{2}
^{229}Th	9.27×10^{-2}	1.01×10^{-1}
^{230}Th	9.00×10^{-3}	9.19×10^{-3}
^{231}Th	4.16×10^{-3}	4.16×10^{-3}
^{232}Th	9.40×10^{-2}	9.40×10^{-2}
^{234}Th	4.78×10^{1}	9.92×10^{-2}
^{231}Pa	6.09×10^{-1}	6.09×10^{-1}
^{233}Pa	6.92×10^{5}	3.01×10^{3}
^{234}Pa	4.78×10^{-2}	9.93×10^{-5}
^{234m}Pa	4.78×10^{1}	9.93×10^{-2}
^{232}U	2.23×10^{2}	2.21×10^{2}
^{233}U	1.54×10^{2}	1.55×10^{2}
^{234}U	3.59×10^{1}	3.60×10^{1}
^{235}U	4.16×10^{-3}	4.16×10^{-3}
^{236}U	3.38×10^{-1}	3.38×10^{-1}
^{237}U	2.28×10^{-1}	-
^{237}Np	6.61×10^{-1}	6.61×10^{-1}
^{239}Np	9.87×10^{0}	9.87×10^{0}
^{236}Pu	5.96×10^{-1}	5.17×10^{-1}
^{238}Pu	1.27×10^{4}	1.27×10^{4}
^{239}Pu	8.98×10^{0}	8.98×10^{0}
^{240}Pu	1.76×10^{1}	1.79×10^{1}
^{241}Pu	7.15×10^{3}	6.95×10^{3}
^{242}Pu	3.47×10^{-1}	3.47×10^{-1}
^{241}Am	1.60×10^{1}	2.26×10^{1}

Table 1 (Contd.)

Isotope	150 Day Cooled (Ci/metric ton)[a]	365 Day Cooled (Ci/metric ton)[a]
^{242}Am	3.94×10^{-1}	3.93×10^{-1}
^{242m}Am	3.94×10^{-1}	3.93×10^{-1}
^{243}Am	2.36×10^{1}	1.54×10^{1}
^{242}Cm	2.21×10^{3}	8.86×10^{2}
^{243}Cm	8.76×10^{0}	8.59×10^{0}
^{244}Cm	4.02×10^{3}	3.94×10^{3}

[a] Curies per metric ton of uranium plus thorium present at the start of irradiation.

The concentration limits according to 10 CFR, Part 20 for 139 isotopes present in HTGR fuel from the Fort St. Vrain Reactor in significant amounts ($> 10^{-8}$ Ci/metric ton) are listed in Table 2. Certain values listed were obtained by using the decay mode and half-life (included in Table 2, for completeness) according to instructions given in 10 CFR, Part 20.

IV. Process Decontamination Factors

A measure of the hazard of an isotope is the quantity of air required to dilute the isotope to the concentration limit shown in Table 2. Use of this dilution as a basis for calculating overall gaseous process decontamination factors has simplicity and relates to the maximum value of the hazard, since no consideration is given to the paths of travel to human beings. The dilution values calculated for 150- and 365-day-cooled fuels are shown in Tables 3 and 4 respectively.

Normalization of the gas dilution required* yields a number that is a measure of the calculated relative gaseous potential hazard (RGPH) of the various isotopes. One isotope (Pu-238) represents 79% of the total calculated isotopic potential hazard (for 150-day-cooled fuel) from the combustion of HTGR fuel elements. Other isotopes that are of major potential hazards are: Cm-244 (6%), Sr-90 (4%), Po-216† (3%), Ce-144 (2%), Po-212† (2%), Pu-241 (1%), and Cs-134 (1%). By contrast, the more volatile isotopes have the following relative gaseous potential hazards: Kr-85 (9×10^{-5}%), I-131 (1×10^{-5}%), H-3 (9×10^{-6}%), I-129 (3×10^{-6}%), C-14 (3×10^{-8}%). It must be remarked that this comparison says nothing about actual amounts contained in the burner off-gas; it compares the isotopes to each other on the basis of the amounts in the fuel elements and permissible discharge limits, i.e., decontamination of a completely vaporized fuel.

Stoichiometric combustion of the graphite associated with 1 metric ton of heavy metal produces a minimum volume (STP) of about 5.2×10^5 ft^3 of carbon dioxide. Reprocessing plant stacks can be designed to give a stack dilution of 5.2×10^{-8}. A 1-metric ton/day HTGR reprocessing plant with such a stack would have a dilution of about 10^{-13} metric ton/ft^3. Multiplication of the values given in Tables 3 and 4 by 10^{-13} metric ton/ft^3 gives the overall gaseous process decontamination factors that must be obtained during the combustion process, i.e., before release from the stack. The overall gaseous process decontamination factors thus calculated are shown in Figures 3-7. Elements with overall gaseous process decontamination factors greater than unity require decontamination prior to release to the stack. It should be noted that, if both the overall gaseous process decontamination factors and the calculated relative gaseous potential hazards of the various isotopes are arranged in descending sequences, a 1:1 correspondence exists as to the location of a given isotope in both sequences.

---

*The normalization is carried out as follows:

$$RGPH_i = \frac{X_i}{\sum_N X_i}$$, where X_i = gas dilution required (ft^3/metric ton) for isotope i.

†Po-216 and Po-212, U-232 daughters, have half-lives of <1 sec; thus a few minutes holdup in the off-gas system eliminates them as potential hazards.

Table 2. Concentration Limits in Air Above Background for Unrestricted Areas as Specified by Appendix B, Table II, Column 1, of 10 CFR Part 20

Isotope	Half-Life[a]	Decay Mode	Chemical[b] Form	Concentration Limit (μCi/ml)
^{3}H	1.2×10^{1} y	β	S,I	2×10^{-7}
^{10}Be	2.5×10^{6} y	β	c	1×10^{-10}
^{14}C	5.6×10^{3} y	β	Sub [d,e]	1×10^{-6}
^{32}P	1.4×10^{1} d	β	S	2×10^{-9}
^{51}Cr	2.8×10^{1} d	γ	S	4×10^{-7}
^{54}Mn	3.0×10^{2} d	γ	S,I	1×10^{-9}
^{55}Fe	2.9×10^{0} y	EC	S,I	3×10^{-8}
^{59}Fe	4.5×10^{1} d	γ	I	2×10^{-9}
^{60}Co	5.3×10^{0} y	γ	I	3×10^{-10}
^{79}Se	6.5×10^{4} y	β	c	1×10^{-10}
^{85}Kr	1.1×10^{1} y	β	Sub[d]	3×10^{-7}
^{86}Rb	1.9×10^{1} d	β	I	2×10^{-9}
^{89}Sr	5.2×10^{1} d	β	S	3×10^{-10}
^{90}Sr	2.8×10^{1} y	β	S	3×10^{-11}
^{90}Y	6.4×10^{1} h	β	I	3×10^{-9}
^{91}Y	5.9×10^{1} d	β	S,I	1×10^{-9}
^{93}Zr	1.5×10^{6} y	β	S	4×10^{-9}
^{95}Zr	6.5×10^{1} d	β	I	1×10^{-9}
^{93m}Nb	1.4×10^{1} y	γ	S	4×10^{-9}
^{95}Nb	3.5×10^{1} d	β	I	3×10^{-9}
^{95m}Nb	9.0×10^{1} h	γ	c	1×10^{-10}
^{99}Mo	6.7×10^{1} h	β	I	7×10^{-9}
^{99}Tc	2.2×10^{5} y	β	I	2×10^{-9}
^{99m}Tc	6.0×10^{0} h	γ	I	5×10^{-7}
^{103}Ru	4.0×10^{1} d	β	I	3×10^{-9}
^{106}Ru	3.7×10^{2} d	β	I	2×10^{-10}
^{103m}Rh	5.7×10^{1} m	γ	I	2×10^{-6}
^{106}Rh	3.0×10^{1} s	β	Sub[d]	3×10^{-8}
^{107}Pd	7.5×10^{6} y	β	c	1×10^{-10}
^{110}Ag	2.4×10^{1} s	β	Sub[d]	3×10^{-8}
^{110m}Ag	2.5×10^{2} d	γ	I	3×10^{-10}
^{111}Ag	7.5×10^{0} d	β	I	8×10^{-9}

Table 2 (Contd.)

Isotope	Half-Life[a]	Decay Mode	Chemical[b] Form	Concentration Limit (μCi/ml)
^{113m}Cd	1.4×10^{1} y	β	c	1×10^{-10}
^{115m}Cd	4.3×10^{1} d	β	S,I	1×10^{-9}
^{117m}Sn	1.4×10^{1} d	γ	c	1×10^{-10}
^{119m}Sn	2.5×10^{2} d	γ	c	1×10^{-10}
^{123m}Sn	1.3×10^{2} d	β	c	1×10^{-10}
^{125}Sn	9.4×10^{0} d	β	I	3×10^{-9}
^{126}Sn	1.0×10^{5} y	β	c	1×10^{-10}
^{124}Sb	6.0×10^{1} d	β	I	7×10^{-10}
^{125}Sb	2.7×10^{0} y	β	I	9×10^{-10}
^{126}Sb	1.3×10^{1} d	β	c	1×10^{-10}
^{126m}Sb	1.9×10^{1} m	β	Sub[d]	3×10^{-8}
^{127}Sb	9.3×10^{1} h	β	c	1×10^{-10}
^{123m}Te	1.2×10^{2} d	γ	c	1×10^{-10}
^{125m}Te	5.8×10^{1} d	γ	I	4×10^{-9}
^{127}Te	9.4×10^{0} h	β	I	3×10^{-8}
^{127m}Te	1.1×10^{2} d	γ	I	1×10^{-9}
^{129}Te	6.9×10^{1} m	β	I	1×10^{-7}
^{129m}Te	3.4×10^{1} d	β	I	1×10^{-9}
^{132}Te	7.8×10^{1} h	β	I	4×10^{-9}
^{129}I	1.7×10^{7} y	β	S	2×10^{-11}
^{131}I	8.1×10^{0} d	β	S	1×10^{-10}
^{132}I	2.3×10^{0} h	β	S	3×10^{-9}
^{129m}Xe	8.0×10^{0} d	γ	c	1×10^{-10}
^{131m}Xe	1.2×10^{1} d	γ	Sub[d]	4×10^{-7}
^{133}Xe	5.3×10^{0} d	β	Sub[d]	3×10^{-7}
^{134}Cs	2.1×10^{0} y	β	I	4×10^{-10}
^{135}Cs	3.0×10^{6} y	β	I	3×10^{-9}
^{136}Cs	1.3×10^{1} d	β	I	6×10^{-9}
^{137}Cs	3.0×10^{1} y	β	I	5×10^{-10}
^{137m}Ba	2.6×10^{0} m	γ	Sub[d]	3×10^{-8}
^{140}Ba	1.3×10^{1} d	β	I	1×10^{-9}
^{140}La	4.0×10^{1} h	β	I	4×10^{-9}
^{141}Ce	3.3×10^{1} d	β	I	5×10^{-9}
^{144}Ce	2.8×10^{2} d	β	I	2×10^{-10}

Table 2 (Contd.)

Isotope	Half-Life[a]	Decay Mode	Chemical[b] Form	Concentration Limit (μCi/ml)
^{143}Pr	1.4×10^{1} d	β	I	6×10^{-9}
^{144}Pr	1.7×10^{1} m	β	Sub[d]	3×10^{-8}
^{147}Nd	1.1×10^{1} d	β	I	8×10^{-9}
^{147}Pm	2.6×10^{0} y	β	S	2×10^{-9}
^{148}Pm	5.4×10^{0} d	β	c	1×10^{-10}
^{148m}Pm	4.2×10^{1} d	β	c	1×10^{-10}
^{151}Sm	8.7×10^{1} y	β	S	2×10^{-9}
^{152m}Eu	9.3×10^{0} h	β, EC	S, I	1×10^{-8}
^{152}Eu	1.2×10^{1} y	β, EC	S	4×10^{-10}
^{154}Eu	1.6×10^{1} y	β	S	1×10^{-10}
^{155}Eu	1.8×10^{0} y	β	S, I	3×10^{-9}
^{156}Eu	1.5×10^{1} d	β	c	1×10^{-10}
^{162}Gd	1.0×10^{0} y	β	c	1×10^{-10}
^{160}Tb	7.2×10^{1} d	β	I	1×10^{-9}
^{161}Tb	6.9×10^{0} d	β	c	1×10^{-10}
^{162m}Tb	2.2×10^{0} h	β	c	1×10^{-10}
^{207}Tb	4.8×10^{0} m	β	c	3×10^{-8}
^{208}Tl	3.1×10^{0} m	β	Sub[d]	3×10^{-8}
^{209}Tl	2.2×10^{0} m	β	c	3×10^{-8}
^{209}Pb	3.3×10^{0} h	β	c	1×10^{-10}
^{211}Pb	3.6×10^{1} m	β	c	3×10^{-8}
^{212}Pb	1.1×10^{1} h	β	S	6×10^{-10}
^{211}Bi	2.2×10^{0} m	α	c	2×10^{-14}
^{212}Bi	6.1×10^{1} m	α, β	S	3×10^{-9}
^{213}Bi	4.7×10^{1} s	α	c	2×10^{-14}
^{212}Po	3.0×10^{-7} s	α	c	2×10^{-14}
^{213}Po	4.2×10^{-6} s	α	c	2×10^{-14}
^{215}Po	1.8×10^{-3} s	α	c	2×10^{-14}
^{216}Po	1.5×10^{-1} s	α	c	2×10^{-14}
^{217}At	1.8×10^{-2} s	α	c	2×10^{-14}
^{219}Rn	3.9×10^{0} s	α	c	2×10^{-14}
^{220}Rn	5.5×10^{1} s	α	S	1×10^{-8}
^{221}Fr	4.8×10^{0} m	α	c	2×10^{-14}
^{223}Fr	2.1×10^{1} m	β	c	3×10^{-8}

Table 2 (Contd.)

Isotope	Half-Life[a]	Decay Mode	Chemical[b] Form	Concentration Limit (μCi/ml)
^{223}Ra	1.2×10^{1} d	α	I	8×10^{-12}
^{224}Ra	3.6×10^{0} d	α	I	2×10^{-11}
^{225}Ra	1.5×10^{1} d	β	c	3×10^{-8}
^{228}Ra	6.7×10^{0} y	β	I	1×10^{-12}
^{225}Ac	1.0×10^{1} d	α	c	2×10^{-14}
^{227}Ac	2.2×10^{1} y	β	S	8×10^{-14}
^{228}Ac	6.1×10^{0} d	β	I	6×10^{-10}
^{227}Th	1.8×10^{1} d	α	c	2×10^{-14}
^{228}Th	1.9×10^{0} y	α	I	2×10^{-13}
^{229}Th	7.3×10^{3} y	α	c	2×10^{-14}
^{230}Th	8.0×10^{4} y	α	S	8×10^{-14}
^{231}Th	2.6×10^{1} h	β	c	1×10^{-10}
^{232}Th	1.4×10^{10} y	α	S,I	1×10^{-12}
^{234}Th	2.1×10^{1} d	β	I	1×10^{-9}
^{231}Pa	3.3×10^{4} y	α	S	4×10^{-14}
^{233}Pa	2.7×10^{1} d	β	I	6×10^{-9}
^{234}Pa	6.7×10^{0} h	β	c	1×10^{-10}
^{234m}Pa	1.2×10^{1} y	β	c	3×10^{-8}
^{232}U	7.2×10^{1} y	α	I	9×10^{-13}
^{233}U	1.6×10^{5} y	α	I	4×10^{-12}
^{234}U	2.5×10^{5} y	α	I	4×10^{-12}
^{235}U	7.1×10^{8} y	α	I	4×10^{-12}
^{236}U	2.4×10^{7} y	α	I	4×10^{-12}
^{237}U	6.8×10^{0} d	β	c	1×10^{-10}
^{237}Np	2.1×10^{6} y	α	S	1×10^{-13}
^{239}Np	2.4×10^{0} d	β	I	2×10^{-8}
^{236}Pu	2.9×10^{0} y	α	c	2×10^{-14}
^{238}Pu	8.6×10^{1} y	α	S	7×10^{-14}
^{239}Pu	2.4×10^{4} y	α	S	6×10^{-14}
^{240}Pu	6.6×10^{3} y	α	S	6×10^{-14}
^{241}Pu	1.3×10^{1} y	β	S	3×10^{-12}
^{242}Pu	3.8×10^{5} y	α	S	6×10^{-14}
^{241}Am	4.6×10^{2} y	α	S	2×10^{-13}
^{242}Am	1.6×10^{1} h	β, EC	S	1×10^{-9}

Table 2 (Contd.)

Isotope	Half-Life[a]	Decay Mode	Chemical[b] Form	Concentration Limit (μCi/ml)
^{242m}Am	1.5×10^{2} y	γ	S	2×10^{-13}
^{243}Am	8.0×10^{3} y	α	S	2×10^{-13}
^{242}Cm	1.6×10^{2} d	α	S	4×10^{-12}
^{243}Cm	3.2×10^{1} y	α	S	2×10^{-13}
^{244}Cm	1.8×10^{1} y	α	S	3×10^{-13}

[a] s ≡ second, m ≡ minute, h ≡ hour, d ≡ day, y ≡ year.

[b] The chemical forms indicated are those with the lowest permissible concentration limit listed in Appendix B, Table II, Column 1, of 10 CFR Part 20. S ≡ soluble, I ≡ insoluble.

[c] Concentration limits for this nuclide are not given in Appendix B, Table II, Column 1, of 10 CFR Part 20. Concentration limits used are based on half-life, decay mode, and chemical form according to Appendix B, Table II, Column 1, of 10 CFR Part 20.

[d] "Sub" means that the values given are for submersion in a semispherical infinite cloud of airborne material.

[e] Concentration limit is for CO_2.

Table 3. Dilution Required per Metric Ton of Heavy Metal for Six-Year-Irradiated FSVR Fuel Calculated According to Appendix B, Table II, Column 1, of 10 CFR Part 20

Gas Dilution Required for 150-day-cooled Fuel

	Isotope	ft³/metric ton		Isotope	ft³/metric ton
1.	^{238}Pu	6.4×10^{18}	33.	^{103}Ru	5.7×10^{14}
2.	^{244}Cm	4.7×10^{17}	34.	^{231}Pa	5.4×10^{14}
3.	^{90}Sr	3.6×10^{17}	35.	^{127m}Te	5.4×10^{14}
4.	^{216}Po [a]	2.3×10^{17}	36.	^{137m}Ba	3.6×10^{14}
5.	^{144}Ce	1.8×10^{17}	37.	^{129m}Te	3.5×10^{14}
6.	^{212}Po [a]	1.5×10^{17}	38.	^{234}U	3.2×10^{14}
7.	^{241}Pu	8.4×10^{16}	39.	^{224}Ra	2.3×10^{14}
8.	^{134}Cs	6.6×10^{16}	40.	^{237}Np	2.3×10^{14}
9.	^{89}Sr	2.8×10^{16}	41.	^{123m}Sn	2.3×10^{14}
10.	^{228}Th	2.3×10^{16}	42.	^{242}Pu	2.0×10^{14}
11.	^{137}Cs	2.3×10^{16}	43.	^{156}Eu	2.0×10^{14}
12.	^{242}Cm	2.0×10^{16}	44.	^{148m}Pm	2.0×10^{14}
13.	^{106}Ru	1.5×10^{16}	45.	^{211}Bi	1.6×10^{14}
14.	^{95}Zr	1.4×10^{16}	46.	^{215}Po	1.6×10^{14}
15.	^{91}Y	1.1×10^{16}	47.	^{219}Rn	1.6×10^{14}
16.	^{240}Pu	1.0×10^{16}	48.	^{229}Th	1.6×10^{14}
17.	^{232}U	8.7×10^{15}	49.	^{227}Th	1.6×10^{14}
18.	^{95}Nb	8.4×10^{15}	50.	^{217}At	1.6×10^{14}
19.	^{239}Pu	5.3×10^{15}	51.	^{225}Ac	1.6×10^{14}
20.	^{154}Eu	4.5×10^{15}	52.	^{213}Bi	1.6×10^{14}
21.	^{243}Am	4.2×10^{15}	53.	^{221}Fr	1.6×10^{14}
22.	^{233}Pa	4.1×10^{15}	54.	^{213}Po	1.6×10^{14}
23.	^{90}Y	3.6×10^{15}	55.	^{155}Eu	1.3×10^{14}
24.	^{95m}Nb	2.9×10^{15}	56.	^{106}Rh	9.7×10^{13}
25.	^{241}Am	2.8×10^{15}	57.	^{242m}Am	7.0×10^{13}
26.	^{147}Pm	2.1×10^{15}	58.	^{125m}Te	6.9×10^{13}
27.	^{243}Cm	1.5×10^{15}	59.	^{227}Ac	4.2×10^{13}
28.	^{233}U	1.4×10^{15}	60.	^{140}Ba	1.8×10^{13}
29.	^{144}Pr	1.2×10^{15}	61.	^{127}Te	1.8×10^{13}
30.	^{236}Pu	1.1×10^{15}	62.	^{148}Pm	1.6×10^{13}
31.	^{125}Sb	7.5×10^{14}	63.	^{124}Sb	1.5×10^{13}
32.	^{141}Ce	6.2×10^{14}	64.	^{110m}Ag	1.4×10^{13}

Table 3 (Contd.)

	Isotope	ft³/metric ton		Isotope	ft³/metric ton
65.	^{151}Sm	1.0×10^{13}	99.	^{129}I	2.4×10^{11}
66.	^{160}Tb	8.3×10^{12}	100.	^{231}Th	1.5×10^{11}
67.	^{212}Pb	7.8×10^{12}	101.	^{237}U	8.0×10^{10}
68.	^{85}Kr	7.7×10^{12}	102.	^{113m}Cd	6.8×10^{10}
69.	^{143}Pr	6.1×10^{12}	103.	^{93}Zr	6.4×10^{10}
70.	^{162m}Tb	5.8×10^{12}	104.	^{234m}Pa	5.6×10^{10}
71.	^{162}Gd	5.8×10^{12}	105.	^{208}Tl	5.6×10^{10}
72.	^{140}La	5.1×10^{12}	106.	^{59}Fe	3.8×10^{10}
73.	^{230}Th	4.0×10^{12}	107.	^{235}U	3.7×10^{10}
74.	^{232}Th	3.3×10^{12}	108.	^{209}Pb	3.2×10^{10}
75.	^{119m}Sn	3.3×10^{12}	109.	^{110}Ag	1.8×10^{10}
76.	^{236}U	3.0×10^{12}	110.	^{239}Np	1.7×10^{10}
77.	^{126}Sb	2.9×10^{12}	111.	^{234}Pa	1.7×10^{10}
78.	^{129}Te	2.2×10^{12}	112.	^{107}Pd	1.7×10^{10}
79.	^{228}Ra	1.9×10^{12}	113.	^{242}Am	1.4×10^{10}
80.	^{234}Th	1.7×10^{12}	114.	^{152m}Eu	1.3×10^{10}
81.	^{212}Bi	1.6×10^{12}	115.	^{93m}Nb	1.2×10^{10}
82.	^{115m}Cd	1.3×10^{12}	116.	^{135}Cs	1.1×10^{10}
83.	^{123m}Te	1.1×10^{12}	117.	^{10}Be	5.3×10^{9}
84.	^{103}Rh	8.5×10^{11}	118.	^{228}Ac	3.2×10^{9}
85.	^{131}I	8.0×10^{11}	119.	^{125}Sn	2.8×10^{9}
86.	^{79}Se	7.5×10^{11}	120.	^{14}C	2.1×10^{9}
87.	^{3}H	7.2×10^{11}	121.	^{126m}Sb	1.4×10^{9}
88.	^{99}Tc	6.0×10^{11}	122.	^{131m}Xe	3.0×10^{8}
89.	^{55}Fe	5.9×10^{11}	123.	^{129m}Xe	2.5×10^{8}
90.	^{220}Rn	4.7×10^{11}	124.	^{211}Pb	1.1×10^{8}
91.	^{126}Sn	4.3×10^{11}	125.	^{207}Tl	1.1×10^{8}
92.	^{223}Ra	4.1×10^{11}	126.	^{225}Ra	1.1×10^{8}
93.	^{136}Cs	3.8×10^{11}	127.	^{117m}Sn	5.5×10^{7}
94.	^{86}Rb	3.5×10^{11}	128.	^{111}Ag	3.9×10^{7}
95.	^{54}Mn	3.2×10^{11}	129.	^{161}Tb	4.9×10^{6}
96.	^{152}Eu	3.2×10^{11}	130.	^{32}P	1.9×10^{6}
97.	^{147}Nd	3.0×10^{11}	131.	^{209}Tl	1.9×10^{6}
98.	^{60}Co	2.5×10^{11}	132.	^{51}Cr	1.0×10^{6}

Table 3 (Contd.)

	Isotope	ft^3/metric ton		Isotope	ft^3/metric ton
133.	^{133}Xe	7.1 x 10^5	136.	^{132}Te	1.5 x 10^2
134.	^{127}Sb	1.4 x 10^5	137.	^{99}Mo	5.2 x 10^{-1}
135.	^{132}I	2.1 x 10^2	138.	^{99m}Tc	7.0 x 10^{-3}

[a] Po-216 and Po-212, U-232 daughters, have half-lives of <1 sec; thus a few minutes holdup in the off-gas system eliminates them as potential hazards.

Table 4. Dilution Required per Metric Ton of Heavy Metal for Six-Year-Irradiated FSVR Fuel Calculated According to Appendix B, Table II, Column 1, of 10 CFR Part 20

Gas Dilution Required for 365-day-cooled Fuel

	Isotope	ft³/metric ton		Isotope	ft³/metric ton
1.	^{238}Pu	6.4×10^{18}	32.	^{234}U	3.2×10^{14}
2.	^{244}Cm	4.6×10^{17}	33.	^{95m}Nb	2.9×10^{14}
3.	^{90}Sr	3.6×10^{17}	34.	^{224}Ra	2.7×10^{14}
4.	^{216}Po [a]	2.7×10^{17}	35.	^{237}Np	2.3×10^{14}
5.	^{212}Po [a]	1.7×10^{17}	36.	^{242}Pu	2.0×10^{14}
6.	^{144}Ce	1.1×10^{17}	37.	^{211}Bi	1.8×10^{14}
7.	^{241}Pu	8.2×10^{16}	38.	^{215}Po	1.8×10^{14}
8.	^{134}Cs	5.4×10^{16}	39.	^{219}Rn	1.8×10^{14}
9.	^{228}Th	2.7×10^{16}	40.	^{227}Th	1.8×10^{14}
10.	^{137}Cs	2.3×10^{16}	41.	^{217}At	1.8×10^{14}
11.	^{240}Pu	1.1×10^{16}	42.	^{225}Ac	1.8×10^{14}
12.	^{106}Ru	9.7×10^{15}	43.	^{213}Bi	1.8×10^{14}
13.	^{232}U	8.7×10^{15}	44.	^{221}Fr	1.8×10^{14}
14.	^{242}Cm	7.8×10^{15}	45.	^{229}Th	1.8×10^{14}
15.	^{239}Pu	5.3×10^{15}	46.	^{213}Po	1.8×10^{14}
16.	^{154}Eu	4.4×10^{15}	47.	^{127m}Te	1.4×10^{14}
17.	^{241}Am	4.0×10^{15}	48.	^{155}Eu	1.0×10^{14}
18.	^{90}Y	3.6×10^{15}	49.	^{242m}Am	6.9×10^{13}
19.	^{243}Am	2.7×10^{15}	50.	^{123m}Sn	6.9×10^{13}
20.	^{147}Pm	1.8×10^{15}	51.	^{106}Rh	6.5×10^{13}
21.	^{89}Sr	1.6×10^{15}	52.	^{125m}Te	6.0×10^{13}
22.	^{243}Cm	1.5×10^{15}	53.	^{227}Ac	4.6×10^{13}
23.	^{233}U	1.4×10^{15}	54.	^{233}Pa	1.8×10^{13}
24.	^{95}Zr	1.4×10^{15}	55.	^{103}Ru	1.3×10^{13}
25.	^{95}Nb	9.7×10^{14}	56.	^{151}Sm	1.0×10^{13}
26.	^{236}Pu	9.1×10^{14}	57.	^{212}Pb	8.9×10^{12}
27.	^{91}Y	8.4×10^{14}	58.	^{110m}Ag	7.8×10^{12}
28.	^{144}Pr	7.2×10^{14}	59.	^{85}Kr	7.4×10^{12}
29.	^{125}Sb	6.5×10^{14}	60.	^{141}Ce	6.3×10^{12}
30.	^{231}Pa	5.4×10^{14}	61.	^{148m}Pm	5.8×10^{12}
31.	^{137m}Ba	3.5×10^{14}	62.	^{127}Te	4.5×10^{12}

Table 4 (Contd.)

	Isotope	ft³/metric ton		Isotope	ft³/metric ton
63.	^{129m}Te	4.4×10^{12}	95.	^{129}Te	2.8×10^{10}
64.	^{230}Th	4.1×10^{12}	96.	^{103m}Rh	2.0×10^{10}
65.	^{152}Gd	3.9×10^{12}	97.	^{239}Np	1.7×10^{10}
66.	^{152m}Tb	3.9×10^{12}	98.	^{107}Pd	1.7×10^{10}
67.	^{232}Th	3.3×10^{12}	99.	^{242}Am	1.4×10^{10}
68.	^{236}U	3.0×10^{12}	100.	^{93m}Nb	1.3×10^{10}
69.	^{228}Ra	2.0×10^{12}	101.	^{152m}Eu	1.2×10^{10}
70.	^{119m}Sn	1.8×10^{12}	102.	^{135}Cs	1.1×10^{10}
71.	^{212}Bi	1.8×10^{12}	103.	^{110}Ag	1.0×10^{10}
72.	^{124}Sb	1.3×10^{12}	104.	^{156}Eu	9.9×10^{9}
73.	^{160}Tb	1.0×10^{12}	105.	^{10}Be	5.3×10^{9}
74.	^{79}Se	7.5×10^{11}	106.	^{234}Th	3.5×10^{9}
75.	^{3}H	7.0×10^{11}	107.	^{228}Ac	3.4×10^{9}
76.	^{99}Tc	6.0×10^{11}	108.	^{14}C	2.1×10^{9}
77.	^{220}Rn	5.4×10^{11}	109.	^{126m}Sb	1.4×10^{9}
78.	^{55}Fe	5.0×10^{11}	110.	^{59}Fe	1.4×10^{9}
79.	^{148}Pm	4.7×10^{11}	111.	^{140}Ba	1.5×10^{8}
80.	^{223}Ra	4.6×10^{11}	112.	^{211}Pb	1.2×10^{8}
81.	^{126}Sn	4.3×10^{11}	113.	^{207}Tl	1.2×10^{8}
82.	^{126}Sb	4.3×10^{11}	114.	^{86}Rb	1.2×10^{8}
83.	^{152}Eu	3.0×10^{11}	115.	^{225}Ra	1.2×10^{8}
84.	^{123m}Te	3.0×10^{11}	116.	^{234m}Pa	1.2×10^{8}
85.	^{129}I	2.4×10^{11}	117.	^{143}Pr	1.1×10^{8}
86.	^{60}Co	2.3×10^{11}	118.	^{140}La	4.5×10^{7}
87.	^{54}Mn	2.0×10^{11}	119.	^{234}Pa	3.5×10^{7}
88.	^{231}Th	1.5×10^{11}	120.	^{209}Tl	2.1×10^{6}
89.	^{113m}Cd	6.6×10^{10}	121.	^{147}Nd	4.5×10^{5}
90.	^{208}Tl	6.4×10^{10}	122.	^{131}I	7.3×10^{3}
91.	^{93}Zr	6.4×10^{10}	123.	^{51}Cr	4.7×10^{3}
92.	^{115m}Cd	4.1×10^{10}	124.	^{131m}Xe	1.0×10^{3}
93.	^{235}U	3.7×10^{10}	125.	^{111}Ag	9.1×10^{-2}
94.	^{209}Pb	3.6×10^{10}			

[a] Po-216 and Po-212, U-232 daughters, have half-lives of <1 sec; thus a few minutes holdup in the off-gas system eliminates them as potential hazards.

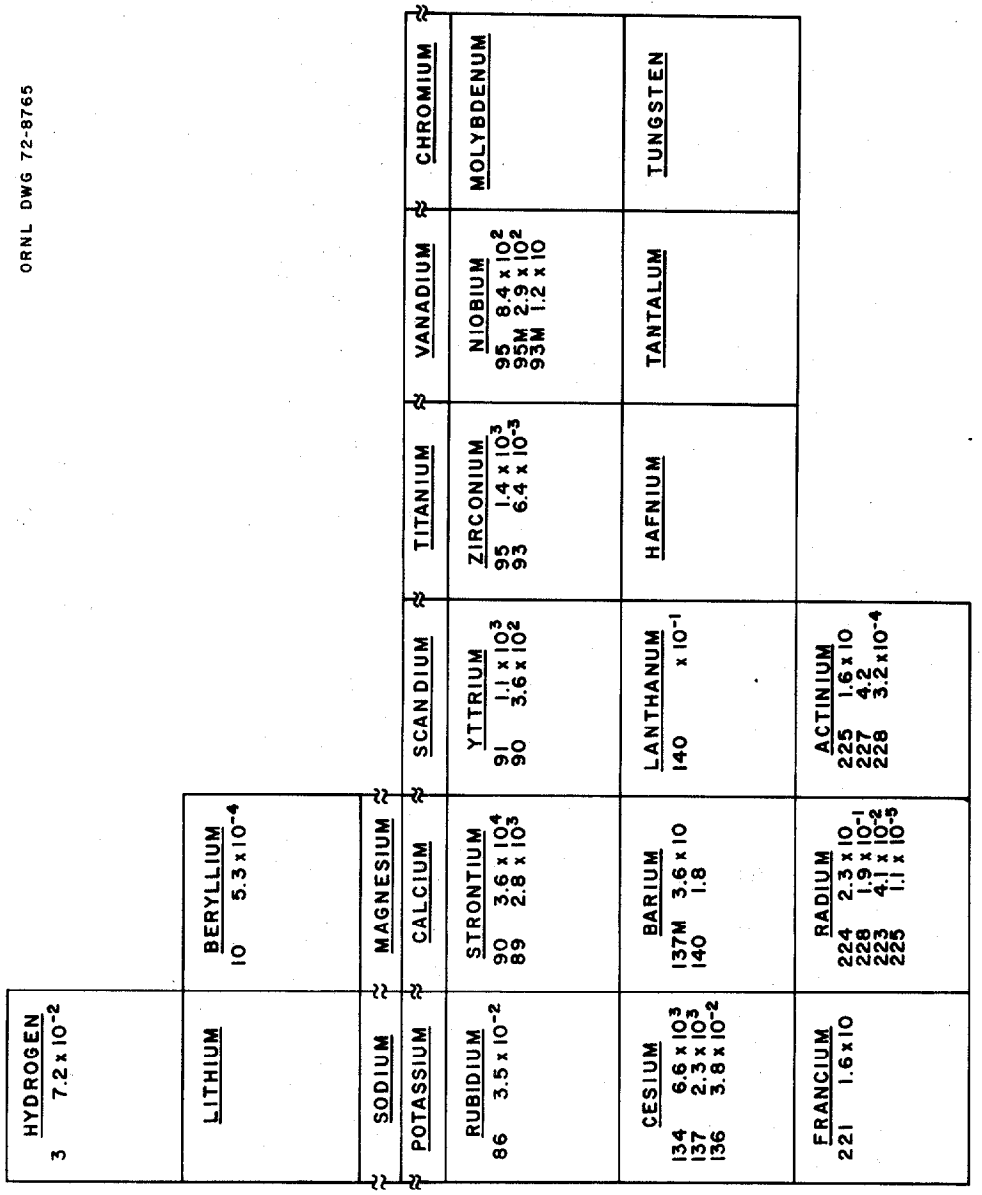

FIGURE 3. GROUPS 1A THROUGH 6B ISOTOPIC GAS-PHASE DECONTAMINATION FACTORS FOR 6-YEAR-IRRADIATED FSVR FUEL ACCORDING TO 10 CFR, PART 20.

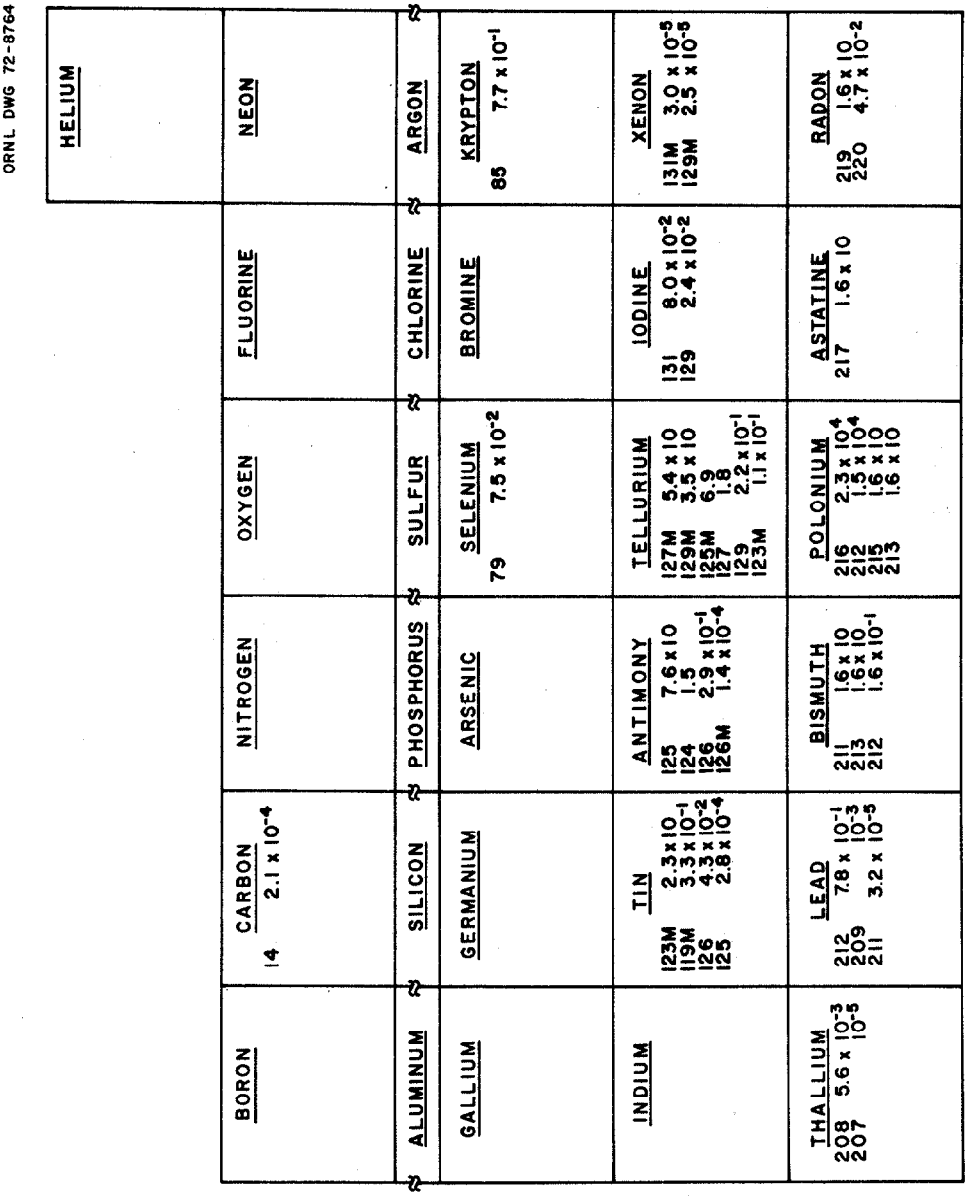

FIGURE 4. GROUPS 3A THROUGH 1G ISOTOPIC GAS-PHASE DECONTAMINATION FACTORS FOR 6-YEAR-IRRADIATED FSVR FUEL ACCORDING TO 10 CFR, PART 20.

ORNL DWG 72-8763

MANGANESE 54 3.2×10^{-2}	IRON 55 5.9×10^{-2} 59 3.8×10^{-3}	COBALT 60 2.5×10^{-2}	NICKEL	COPPER	ZINC
TECHNETIUM 99 6.0×10^{-2}	RUTHENIUM 106 1.5×10^{3} 103 5.7×10	RHODIUM 106 9.7 103M 8.5×10^{-2}	PALLADIUM 107 1.7×10^{-3}	SILVER 110M 1.4 110 1.8×10^{-3}	CADMIUM 115M 1.3×10^{-1} 113M 6.8×10^{-3}
RHENIUM	OSMIUM	IRIDIUM	PLATINUM	GOLD	MERCURY

FIGURE 5. GROUPS 7B THROUGH 2B ISOTOPIC GAS-PHASE DECONTAMINATION FACTORS FOR 6-YEAR-IRRADIATED FSVR FUEL ACCORDING TO 10 CFR, PART 20.

ORNL DWG 72-8762

CERIUM 144 1.8×10^{4} 141 6.2×10	PRASEODYMIUM 144 1.2×10^{2} 143 6.1×10^{-1}	NEODYMIUM 147 3.0×10^{-2}	PROMETHIUM 147 2.1×10^{2} 148M 2.0×10 148 1.6	SAMARIUM 151 1.0	EUROPIUM 154 4.5×10^{2} 156 2.0×10 155 1.3×10 152Y 3.2×10^{-2} 152H 1.3×10^{-3}	GADOLINIUM 162 5.8×10^{-1}
TERBIUM 160 8.3×10^{-1} 162M 5.8×10^{-1}	DYSPROSIUM	HOLMIUM	ERBIUM	THULIUM	YTTERBIUM	LUTETIUM

FIGURE 6. LANTHANIDE ISOTOPIC GAS-PHASE DECONTAMINATION FACTORS FOR 6-YEAR-IRRADIATED FSVR FUEL ACCORDING TO 10 CFR, PART 20.

ORNL DWG 72-8761

THORIUM	PROTACTINIUM	URANIUM	NEPTUNIUM	PLUTONIUM	AMERICIUM	CURIUM
228 2.3×10^{3}	233 4.1×10^{2}	232 8.7×10^{2}	237 2.3×10	238 6.4×10^{5}	243 4.2×10^{2}	244 4.7×10^{4}
229 1.6×10	231 5.4×10	233 1.4×10^{2}	239 1.7×10^{-3}	241 8.4×10^{3}	241 2.8×10^{2}	242 2.0×10^{3}
227 1.6×10	234M 5.6×10^{-3}	234 3.2×10		240 1.0×10^{3}	242M 7.0	243 1.5×10^{2}
230 4.0×10^{-1}	234 1.7×10^{-3}	236 3.0×10^{-1}		239 5.3×10^{2}	242 1.4×10^{-3}	
232 3.3×10^{-1}		237 6.0×10^{-3}		236 1.1×10^{2}		
234 1.7×10^{-1}		235 3.7×10^{-3}		242 2.0×10		
231 1.5×10^{-2}						

BERKELIUM	CALIFORNIUM	EINSTEINIUM	FERMIUM	MENDELEVIUM	NOBELIUM

FIGURE 7. ACTINIDE ISOTOPE GAS-PHASE DECONTAMINATION FACTORS FOR 6-YEAR-IRRADIATED FSVR FUEL ACCORDING TO 10 CFR, PART 20.

V. Conclusions

The simple procedure of comparing the various isotopes present in HTGR fuel elements at reprocessing time on the basis of the amount of air required to dilute each isotope to meet existing gaseous effluent regulations provides a helpful way of understanding which isotopes are likely to become major problems during the actual burning of spent fuel elements. Isotopes with the larger calculated dilution volumes will require larger overall process decontamination factors in order to meet the existing gaseous effluent regulations. The nonvolatile isotopes will have very large decontamination factors for the burning process.

The amount of air required to dilute the Pu-238 contained in a metric ton (preirradiation) of spent HTGR fuel is approximately twenty times that required for diluting Sr-90. By way of comparison, the amount of water required to dilute the Pu-238 is 0.25% of that required to dilute the Sr-90[3]. Thus, consideration of only the isotopes that are known to be of major importance in liquid effluents plus those that are highly volatile is insufficient for identifying potential problems to be encountered in decontaminating the burner off-gas.

If a researcher multiplies the calculated dilution volumes by the relative volatilities (assume rare gases = 1), then he can arrange the isotopes in a sequence that will be representative of the actual relative hazards of the isotopes contaminating the carbon dioxide. Such a sequence would be of invaluable aid in trying to develop a burner off-gas decontamination process.

VI. References

1. M. J. Bell, ORIGEN - The ORNL Isotope Generation and Decay Code, ORNL-4628 (in preparation).

2. R. C. Dahlberg, R. F. Turner, and W. V. Goeddel, "Fort Saint Vrain Core Design Characteristics," Nuclear Engineering International 14 (No. 163), 1073-77 (December 1969).

3. J. W. Snider, unpublished calculations, Oak Ridge National Laboratory.

DISCUSSION

ISBIN: When you present the information in this form, aren't you opening yourself to a considerable amount of criticism from the standpoint that you have not taken into account Part 20 and its fullest implications? Aren't you misinterpreting Part 20 in the implications of this paper?

SNIDER: This paper did not account for the total releases that are permissible in a plant according to Part 20.

ISBIN: Part 20 includes deposition and reconcentration. You would have to go through these calculations for each one of the isotopes to determine whether or not the concentration limits which you took first were applicable.

SNIDER: I have considered only what can be released at the boundary of the plant.

DETERMINATION OF THE RADIOACTIVE NUCLIDES PRESENT IN THE OFF-GAS STREAMS GENERATED BY THE HEAD-END STEPS IN REPROCESSING HTGR TYPE FUELS*

R. S. Lowrie, C. L. Fitzgerald and V. C. A. Vaughen
Oak Ridge National Laboratory
Oak Ridge, Tennessee

Abstract

Results of studies to determine the behavior of radioactive nuclides in the gaseous waste streams generated during the reprocessing of spent High Temperature Gas-Cooled Reactor (HTGR) fuel are presented. The fuel is in the form of coated particles of uranium and thorium, bonded into fuel sticks, and inserted into holes in large hexagonal graphite blocks. Spent fuel is reprocessed to recover the bred ^{233}U and the unburned ^{235}U.

Studies were performed on a small scale in a hot-cell using a generalized head-end reprocessing flowsheet. The fuel specimens were crushed and burned to remove as much graphite as possible, and the burner residue was separated into appropriate size fractions. Those fractions containing TRISO-coated particles were then ground to break the SiC coating and burned a second time. Residues from each fraction, consisting of the uranium/thorium kernels, were leached with acid Thorex reagent. The off-gas from each step was collected and analyzed.

Preliminary tests, primarily to measure ^{85}Kr and tritium release, were made using Dragon fuel compacts containing either BISO-coated $(U\text{-}Th)O_2$ sol-gel particles or both TRISO-coated ThC_2 and TRISO-coated UC_2 particles. Burning the BISO-coated $(U\text{-}Th)O_2$ particles released the bulk of the ^{85}Kr (97-98%) and the tritium (98-99%); the remainder was released during the leaching step. The initial burning of the mixed TRISO-coated ThC_2 and TRISO-coated UC_2 fuel released $\sim$7.4% of the ^{85}Kr. Subsequent grind-burn steps released an additional 7.4% of the ^{85}Kr from the ThC_2 particles and 84.5% from the UC_2 particles.

Experiments with the Recycle Test Element (RTE) fuel specimens are designed to permit sampling the off-gas stream for both volatile and entrained fission products. Tests have been completed on a fuel specimen which contained TRISO-coated fertile ThC_2 particles and TRISO-coated fissile UC_2 particles, and which had been irradiated in the Peach Bottom Reactor. The initial burning released 20% of the tritium and less than 1% of the ^{85}Kr. Most of the tritium and ^{85}Kr in the fertile particles was released during the grinding step, with the remainder being released in the subsequent burning and leaching step. Grinding the fissile particles released most of the ^{85}Kr; the subsequent burning and leaching steps released the tritium and remaining ^{85}Kr. About 3.5% of the gross gamma activity present in the fuel stick was carried over by the off-gas streams during the burning tests; this activity was associated with a variety of both volatile and entrained fission products. Although the primary sintered metal filters collected most of this material, $\sim$1% of the amount carried-over passed through the filter.

---

* Research sponsored by the U. S. Atomic Energy Commission under contract with the Union Carbide Corporation, Oak Ridge, Tennessee.

Although much more work needs to be done, particularly with higher burnup fuels and other fuel particle combinations, some general conclusions can be drawn. Most (98%) of the tritium and ^{85}Kr present in spent HTGR fuel will be released during the grind-burn steps in the head-end operations, although the amounts released during grinding or burning will depend on the kind of fuel particle being processed. Further, small amounts of fission products do pass the primary sintered metal filter and may have to be removed by other means.

Introduction

A knowledge of the potential release of contamination to the environment is an essential part of the siting and hazard evaluation for any plant handling radioactive material. Studies are being performed at the Oak Ridge National Laboratory to determine the behavior of radioactive nuclides during the reprocessing of spent High Temperature Gas-Cooled Reactor (HTGR) fuel. This paper is primarily concerned with the contaminants in the off-gas streams that are generated by the head-end reprocessing steps.

The fuel cycle for the HTGRs, such as those currently being sold by Gulf Energy and Environmental Systems, begins with a fuel containing thorium and ^{235}U. The thorium is converted to ^{233}U and, when steady state of fuel recycle has been reached, about half of the fissile material required for refueling is provided by the ^{233}U. Reprocessing the spent fuel will recover this ^{233}U together with some of the remaining ^{235}U. The fuel is in the form of microspherical particles, bonded into fuel sticks, and inserted into large hexagonal graphite blocks approximately 31.2 in. long and 14.2 in. across the flats as shown in Fig. 1. The fuel particles consist of kernels of thorium or uranium in either the oxide or carbide form with either a BISO or a TRISO protective coating.

> A BISO coating consists of an inner porous carbon buffer layer enveloped by an outer isotropic pyrocarbon layer. A TRISO coating consists of the inner porous carbon buffer layer and two isotropic pyrocarbon layers separated by a thin SiC layer.

Fuel elements may contain all BISO-coated fuel particles, all TRISO-coated particles, or mixtures of both types of particles. Thus, in the Ft. St. Vrain reactor both the fertile (thorium dicarbide) particles and the fissile (uranium dicarbide) particles are TRISO-coated, whereas only the fissile particles will be TRISO-coated in the considerably larger, 1100 MW, power reactors.

The head-end steps in the HTGR fuel reprocessing flowsheet first spearate the fuel particles from the block graphite, then separate fertile from fissile particles and, finally, puts the thorium and uranium into an aqueous solution. This solution is then sent to the solvent extraction step where the uranium-thorium separation and decontamination from fission products is effected. In the reference flowsheet, the fuel element is first crushed, and the crushed material is then burned to eliminate as much graphite as possible. During this step, BISO coatings are burned away, and the uranium/thorium kernel is exposed. Because of the high resistance of SiC to chemical attack, only the outer graphite coating of the TRISO particles burn away. The "burned TRISO" particles must be crushed to break the SiC coating, and then burned a second time to eliminate the inner graphite layers; thus exposing the uranium/thorium kernel. As a final step in all instances, the exposed kernels are leached with acid-thorex reagents (13 $\underline{M}$ HNO_3, 0.05 $\underline{M}$ F^-, 0.1 $\underline{M}$ $A\ell^{+++}$) to dissolve the uranium and thorium. The particular series of head-end steps used thus depends on the TRISO-BISO particle combination present in the fuel element to be processed.

HEX BLOCK FUEL ELEMENT

TRISO-II COATED PARTICLE

Fig. 1. HTGR Fuel

Experimental Equipment

The reprocessing studies are carried out in a hot cell using irradiated fuel specimens weighing 10 to 25 grams. The burning steps are performed in a stainless steel (Type 304) miniburner-filter assembly (Fig. 2). The burner body is placed in a vertical furnace which both furnishes the heat and supports the assembly. The filter holder, which has an independent heating system, will accommodate two sintered metal filters. Burner temperatures are controlled by varying either the oxygen content or the flow rate of the inlet gas stream. In-line infra-red analyzers monitor the off-gas CO and CO_2 content and a 400 channel analyzer monitors the ^{85}Kr concentration. Standard sieves are used for fuel particle separations. A Waring blender, with the bowl modified by installing a purge gas inlet and outlet, is used to grind the TRISO particles and break the SiC layer.

Experimental Results

The hot cell experiments can be divided into two groups, based on the source of the irradiated fuel specimens. The earlier group of experiments utilized fuel compacts obtained through the courtesy of the Dragon Reactor project. The current and continuing group of experiments utilize fuel specimens obtained from a series of Recycle Test Elements (RTE) being irradiated in the Peach Bottom Reactor. Most of the candidate fuel particle combinations are included in these test elements.

The tests made with the Dragon compacts were designed primarily to obtain information on the behavior of the fuel particles in the head-end step, so the fission gas determinations involved only the ^{85}Kr and, in some tests, the tritium content of the off-gas, that is, as generated by each phase of the head-end step. We have completed the experimental work on Dragon compact 413-7-22, which contained BISO-coated sol-gel $(U\text{-}Th)O_2$ particles prepared at ORNL, and on compact 19M, which contains a combination of large TRISO-coated ThC_2 fertile particles and smaller TRISO-coated UC_2 fissile particles. The 413-7-22 compact was crushed, then separated into two samples which were burned, and the burner residues then leached, in duplicate experiments. The bulk of the ^{85}Kr (96.96% and 97.97% of the Kr in each of the respective samples) and of the tritium (98.27% and 99.20%) was released during the burning step; the remainder reported to the off-gas that was generated during the leaching step.

A different experimental procedure was used for the 19M compact. First, the compact was crushed; then it was divided into two samples which were burned in duplicate experiments. The burner ash from each experiment was sieved into a fertile particle fraction (+20 mesh), a fissile particle fraction (-20, +42 mesh) and a fine fraction (-42 mesh) that contained the Al_2O_3 bed material plus broken particles. Each fertile and fissile fraction was ground, burned, and the residue leached; the fines residue was only leached. Only the ^{85}Kr release data are available (Table 1).

In this test, 7.35% of the total ^{85}Kr found was released during the initial burning, and 0.57% was released during the leaching of the fines fraction. Most of the ^{85}Kr in the fertile fraction was evolved in about equal amounts during the grinding step (3.77% of the total Kr) and the burning step (3.63%). Grinding the fissile fraction released 75.48% of the ^{85}Kr with most of the remainder (9.02%) reporting to the burner off-gas.

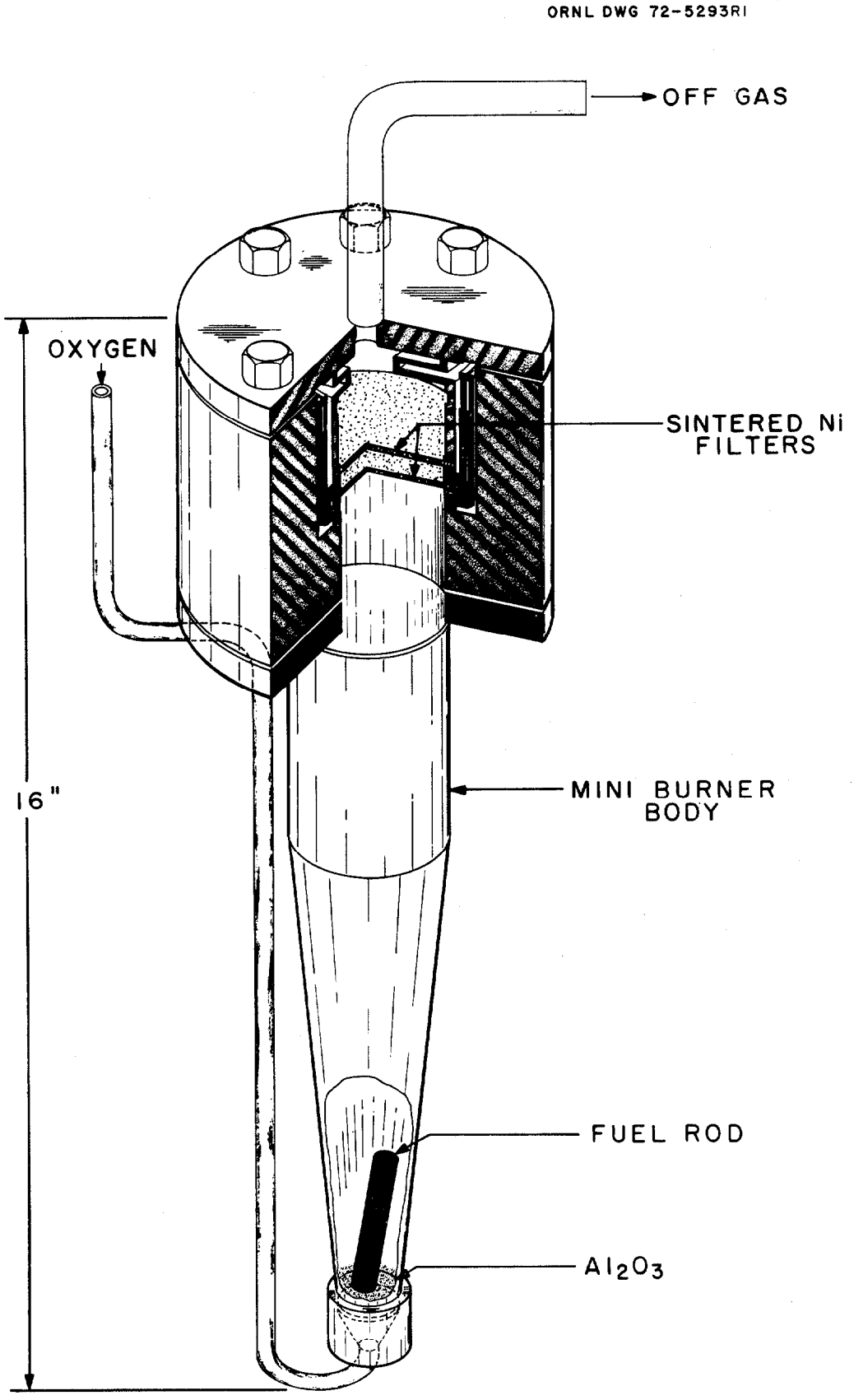

Fig. 2. Miniburner-Filter Assembly

Table 1. ^{85}Kr Release During the Processing of an Irradiated 19-M Dragon Compact with ThC_2 TRISO - UC_2 TRISO Fuel Particles

Operation	^{85}Kr Release (% of total)
Initial Burning	7.35
Residue leach (-42 mesh)	0.57
Fertile fraction (+20 mesh)	
Grinding	3.77
Burning	3.63
Leaching	0.06
Fissile fraction (+42 mesh)	
Grinding	75.48
Burning	9.02
Leaching	0.10

Experiments with the Recycle Test Element fuel specimens were more comprehensive than those with the Dragon compacts and were designed to permit sampling of the burner off-gases for both volatile and entrained fission products. Figure 3 shows a schematic flow diagram of the off-gas sampling train. The off-gas from the burner first passes through two 20μ porosity, sintered Ni filters, held at 500°C (900°F); then, after cooling, it passes into the Fiber Filter holder containing four grades of fibrous filter media. The filtered gas stream passes into a 6 M HCl (refluxing) scrubber, then into a cold (cell temperature) 4 M NaOH scrubber. The gas leaving the NaOH scrubber is dried, filtered to remove desiccant dust, and passed through the in-line ^{85}Kr, CO and CO_2 monitors. It is finally caught in the gas collection bag.

Experimental work has been completed on the first irradiated fuel specimen from RTE-7. The fuel stick (0.5-in.-diam x 2-in.-long) contained TRISO-coated ThC_2 fertile particles and TRISO-coated UC_2 fissile particles and had been in the Peach Bottom Reactor for 252 effective full power days; it had then cooled for 236 days before the experiment started. The fuel stick was placed in the mini-burner on an Al_2O_3 bed and burned (initial burn) to remove the binder carbon and outer pyrolytic carbon coatings. The burner residue was separated into three fractions: a fertile fraction consisting of all particles greater than 42 mesh, a fissile fraction containing all particles less than 42 mesh but greater than 80 mesh, and a minus 80 mesh fines fraction consisting of the Al_2O_3 bed material and broken particles. The fertile and fissile fractions were ground to break the SiC coating, burned, and the burner residue leached; the fines fraction was only leached.

The fission gas release for all grind, burn, and leach steps is shown in Table 2. About 20% of the total tritium and less than 1% of the ^{85}Kr were released during the initial burning. Most of the tritium and about half of the ^{85}Kr associated with the fertile particle fraction was released during the grinding step; the remainder came off during the subsequent burning and leaching steps. Grinding the fissile particle fraction released most of the ^{85}Kr and very little of the tritium. The burning step released most of the remaining ^{85}Kr and a little more tritium. Most of the remaining tritium and ^{85}Kr was released during a 12 hr (750°C) "soaking" period in an oxygen atmosphere. A small amount of tritium and ^{85}Kr (from broken particles) was released when the fine fraction was leached. In essence, 98+ percent of the tritium and ^{85}Kr were released during the grinding and burning steps and will be found in the combined carbon dioxide rich (90%) off-gas stream.

The distribution of other fission products along the off-gas train for the initial burn, the fertile particle fraction burn, and the fissile particle fraction burn is shown in Table 3. About 3.5% of the gross gamma activity present in the fuel stick was carried over by the off-gas streams. Six isotopes, ^{95}Zr, ^{95}Nb, ^{106}Ru, ^{134}Cs, ^{137}Cs, and ^{144}Ce accounted for ∿90% of this activity. Fission products were found on the metallic filter, on the fiber filters and in the scrubber solutions.

The off-gas from the initial burn was only filtered through one sintered Ni filter. The high percentage of ^{134}Cs (19.8%) and ^{137}Cs (14.3%) found on the filter apparently came from surface contamination rather than from broken fuel particles. The amount of activity found on the off-gas train after the fertile particle burn was less than 1% of the total activity carried over, in part due to the fact that the fertile particles only contribute 1 to 2 % to the total fission product content of the fuel stick. Most of the activity which was carried over during the fertile particle burn passed through the filters and was found in the scrubber solutions. The filters were much more effective during the fissile particle burn. Most of the activity carried over during the fissile particle burn was found on the sintered metal filters. Nevertheless, small amounts of activity passed through the filters and were found in the scrubber solutions.

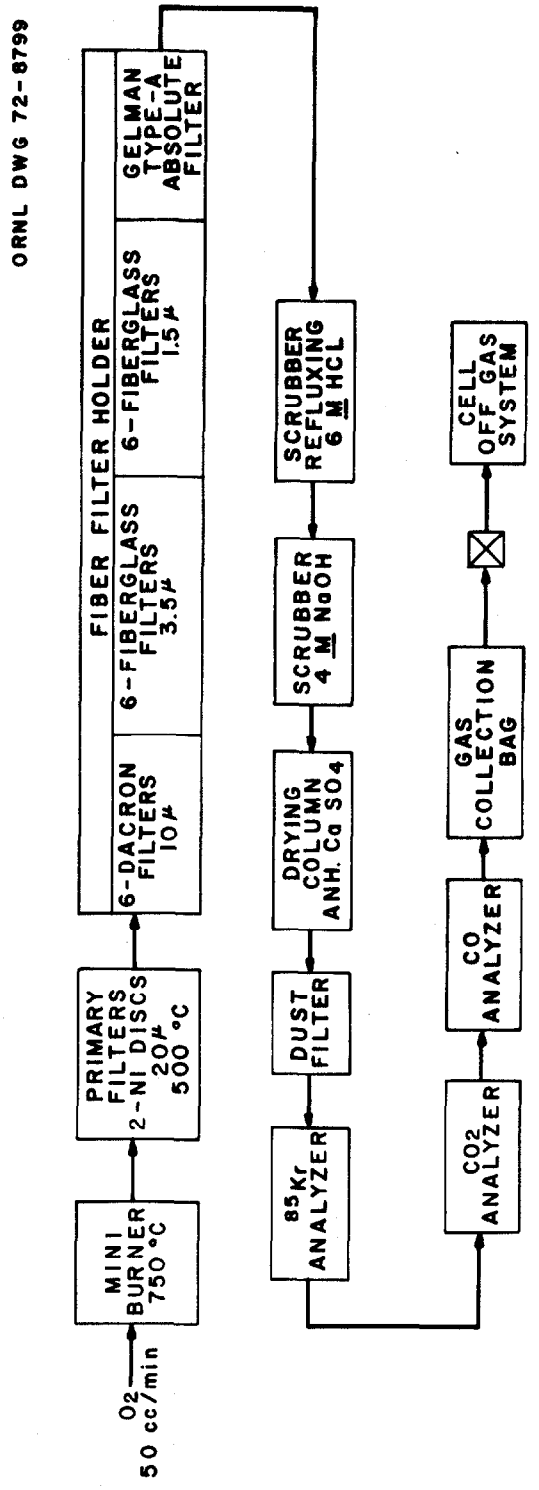

Fig. 3. Off-Gas Train Used for RTE-7 Hot Cell Test

Table 2. Fission Gas Release for RTE-7 ThC_2 TRISO-UC_2 TRISO Fuel

Operation	Percent of Total ^{3}H Released	Percent of Total ^{85}Kr Released
Initial burn	20.562	0.135
Fertile (+42 mesh) fraction		
Grind	33.771	1.263
Burn	2.685	0.989
Leach	0.008	0.106
Total	36.464	2.358
Fissile (+80 mesh) fraction		
Grind	1.431	70.072
Burn[a]	4.594	25.696
Soak[b]	35.803	1.565
Leach	0.042	0.091
Total	41.870	97.424
Fines (-80 mesh) fraction		
Leach	1.104	0.083

[a]Three-hour active burning period.

[b]Held for 12 hr at 750°C after completion of burning.

Table 3. Distribution of Fission Products in the Off-Gas Trains from RTE-7 Tests

Percent of total carry-over during	Gγ (%)	^{95}Zr (%)	^{95}Nb (%)	^{106}Ru (%)	^{134}Cs (%)	^{137}Cs (%)	^{144}Ce (%)
Initial burn	7.91	0.052	0.019	0.534	19.82	14.34	0.081
Fertile fraction burn							
Metal filter-1	0.0261	0.006	0.007	0.107	0.029	0.019	0.008
Metal filter-2	0.0007	0.0001	0.0001	0.003	0.001	0.0006	0.0006
Fiber filters	---	---	---	0.010	0.0003	0.0002	0.0001
Acid scrub	0.720	---	---	---	0.519	0.989	0.010
Base scrub	0.100	0.004	0.0009	0.011	0.243	0.188	0.007
Subtotal	0.850	0.01	0.008	0.131	0.794	0.196	0.026
Fissile fraction burn							
Metal filter-1	85.11	82.81	88.40	75.20	73.09	77.90	82.79
Metal filter-2	5.96	17.03	11.32	23.98	6.07	6.24	16.98
Fiber filters	---	0.001	---	0.182	0.0005	0.0002	0.0006
Acid scrub	0.05	0.024	0.087	0.039	0.042	0.033	0.060
Base scrub	0.10	0.007	0.005	0.010	0.240	0.178	0.007
Subtotal	91.23	99.872	99.812	99.339	79.410	84.454	99.888

Conclusions

Much more work needs to be done, particularly with higher burnup fuels and other fuel particle combinations, before the fission gas release and fission product carry-over patterns are fully characterized. However, some general conclusions can be drawn: Most of the ^{85}Kr (98%) present in HTGR fuels is easily released during the burning and grinding steps. While 98-99% of the tritium will be released during the burning and grinding steps, the tritium release rates during burning may be slower than those for ^{85}Kr, thus requiring longer processing time. Finally, small amounts of fission products do pass through the sintered metal filters and may have to be removed by other means.

DISCUSSION

WITTE: I notice that on the krypton release, the figures don't add up to 100%. Where did the rest go? You showed us some figures which went up to four decimal places; how did you compute such exact numbers?

LOWRIE: The figures do not add up to 100% primarily because of rounding-off errors and other errors in the analysis. As to the very small amounts, this is a calculation with a computer and, therefore, you can get a long string of figures. I think the major thing you need to realize is that they just show trends. You should not put a great deal of reliance on the accuracy of the total amounts at this particular time. Primarily because this is, as I said, a fuel stick which had been irradiated to only a fourth of normal total burnup and, therefore, you can expect to see better figures come along later.

LASER: We have had experience burning HTGR fuel elements. We agree with you that nearly all the krypton and tritium are emitted in fuel burning. Additionally, we have found ruthenium, cesium, cerium and selenium-75 emission. Ruthenium release was 0.01% of the ruthenium that was present; cesium release was approximately 2.2%, and that of cerium was 0.01%. With oxide fuel elements, krypton and tritium emissions were in the range of 10 to 50%. Krypton emission was approximately 8%; ruthenium, 0.003%; cesium, approximately 0.5%; and cerium, 0.003%.

LOWRIE: Thank you, Dr. Laser. We have been watching your experiments in Germany. We are happy to see that our figures are correlating at least reasonably well with yours.

AN INORGANIC ADSORBER MATERIAL FOR OFF-GAS CLEANING IN FUEL REPROCESSING PLANTS

J.G. Wilhelm and H. Schüttelkopf

Radiation Protection and Safety Department/Chemistry
Karlsruhe Nuclear Research Center, Karlsruhe, Federal Republic of Germany

Abstract

An inorganic iodine adsorber material on the basis of $AgNO_3$-impregnated, amorphous silicic acid was developed for use in off-gas cleaning systems of fuel reprocessing plants.

Extensive experimental work was performed to evaluate the removal efficiency of this material from off-gas containing NO_2 for elemental iodine and methyl iodide. Experimental data are given on the influence exerted by relative humidity, temperature, amount of NO_2 in the off-gas, granule size of the adsorber material, and iodine loading, on the performance of the inorganic iodine adsorber material. Also some data will be given on this material concerning the iodine loading capacity and desorption behaviour of iodine at high temperature. The extent and consequences of isotopic exchange between iodine in the form of AgI on the surface of the inorganic adsorber material and iodine in the gas phase will be briefly discussed with respect to the performance time of the adsorber material; also the effects of radiation exposure are indicated.

Moreover, data will be furnished on the removal efficiency of the inorganic adsorber material in the real off-gas of a fuel reprocessing plant; the operating conditions of full-sized iodine filters for fuel reprocessing plants and the price for off-gas cleaning with the inorganic adsorber material will be discussed.

I. Introduction

Adsorber materials are needed for the removal of fission product iodine from the off-gas reprocessing plants. These materials should be resistant against NO_x and higher temperatures because condensation of nitrous and nitric acid has to be avoided. For use in the reprocessing of short cooled fuel, the adsorber materials should be resistant against irradiation up to high doses. Because the bulk amount of the fission product iodine on the adsorber material will be ^{129}I, the final chemical compound of the adsorbed iodine should be resistant against chemical decomposition and provide an extremely low vapour pressure. The loaded adsorber material should be in a form ready for final waste disposal.

The iodine removal efficiencies needed today will be between 90 and 99,9 %, depending on cooling time of the fuel, the capacity of the reprocessing plant and the local conditions. For short cooled fuel, an overall decontamination factor between 10^6 and 10^8 will be needed.

The total release of iodine to the off-gas (before filtering) from a reprocessing plant may be several 10 % of the inventory of the fuel, therefore the iodine adsorber material has to provide a high loading capacity. The results of first tests on different inorganic adsorber materials are given earlier [1, 2]. The inorganic adsorber materials for which data are reported here are composed of amorphous silicic acid. They have a broad spectrum of pores and a porosity of 700 (KTB) and 980 mm^3/g (KTC). The surface area (BET) is 110 (KTB) and 185 m^2/g (KTC), the granule size 1 - 2 mm. Of all impregnating compounds tested, only $AgNO_3$ provided useful decontamination factors. Impregnations between 60 and 80 mg Ag/g KT-material were used normally. The $AgNO_3$-impregnated KTB-material (Ag-KTB) is now available from Bayer in Leverkusen, Germany, under the preliminary product number AC 6120. The removal efficiencies of Ag-KTB and Ag-KTC are approximately the same (with the same amount of $AgNO_3$-impregnation). Because the KTB-material has higher mechanical strength and abrasion resistance, the final selection for use in reprocessing plants is Ag-KTB.

II. Performance of Ag-KT Materials as a Function of Different Operational Parameters

Penetration of CH_3I through Ag-KTC Filter Beds as a Function of the Relative Humidity

The removal efficiency of all iodine adsorbers, especially for CH_3I, is strongly dependent on the relative humidity of the sweep gas. In Fig. 1 the penetration of CH_3I through test beds of Ag-KTC is given as a function of relative humidity and bed depth. For lower bed depth and higher penetration, the plot shows a slight S-shape; in the region of penetrations $< 10^{-2}$ % there are obviously effects from a penetrating impurity which superimposes this effect.

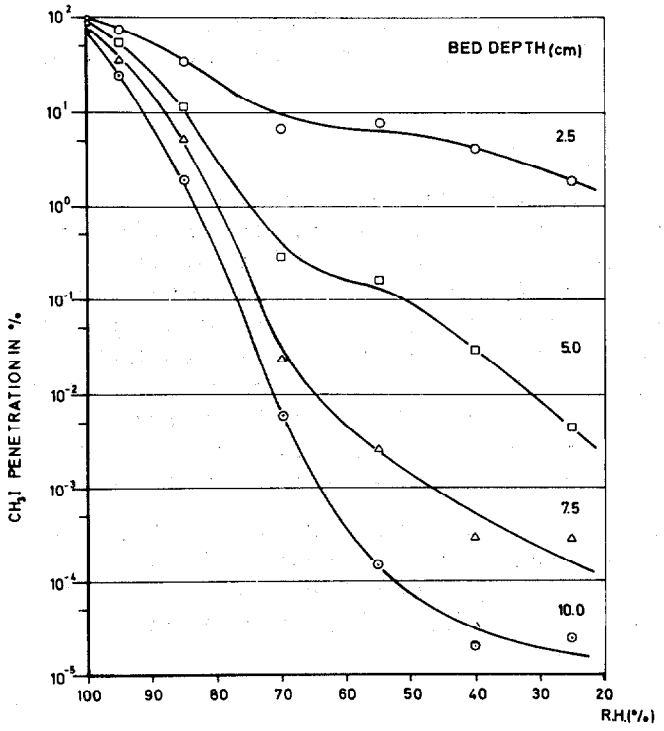

Fig.1 Penetration of CH_3I through Ag-KTC as a function of the relative humidity

The test conditions for all experiments represented in Fig. 1 are:

Sweep gas: Air of atmospheric pressure and 30°C, superficial air velocity 15 m/min. Duration of air flow: Pre-humidification $\geq$ 22 h, CH_3I-injection: 1 h, air flow continued for additional $\geq$ 20 h. The specific loading was 1.5 $\pm$ 0.5 mg/g Ag-KTC, calculated for 10 cm bed depth.

From Fig. 1 the conclusion can be drawn that for economical reasons the relative humidity should be limited to approximately 70 % for the use of Ag-KT materials. This can easily be provided by heating of the off-gas stream.

Influence on the Removal Efficiency Exerted by Temperature

In reprocessing plants mostly washers are provided to recover part of the NO_2. To avoid condensation of water and acid on the surface of the adsorber material, the off-gas has to be heated. A series of experiments with wet air, dew point at 30°C, and addition of 10 % NO_2 to the sweep gas were performed in the temperature region from 80 - 200°C. The data indicated an increase of the removal efficiency for CH_3I between 80 and 125°C. Between 125°C and 175°C no change of removal efficiency with temperature was detectable, at 200°C a slight increase in removal efficiency was recognized. For practical reasons (energy for off-gas heating, choice of material for gaskets etc.) a temperature of 150°C was chosen as operating temperature for a reprocessing plant iodine filter.

Penetration of Ag-KTB Filter Beds as a Function of NO_2-Concentration in the Sweep Gas

Fig. 2 shows the penetration of CH_3I through Ag-KTB as a function of the NO_2-concentration in air for different filter bed depths. At the test temperature of 150°C, there is only a small influence in the region between 1 % and 10 % NO_2. This seems to be important, because their will be a wide variation of the NO_x-content in the dissolver off-gas from a reprocessing plant. To show the exact experimental data, the differential and integral removal efficiencies and the complete experimental conditions are given in Tab. I.

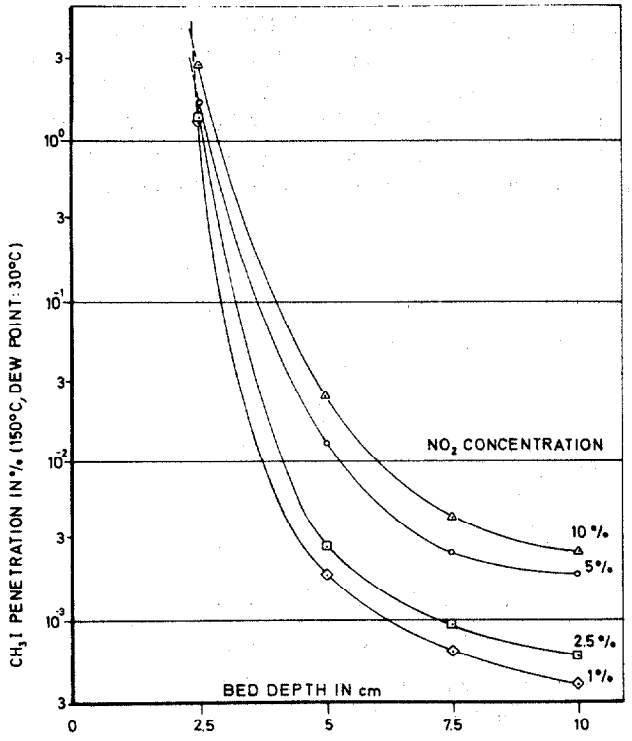

Fig.2 Penetration of CH_3I through Ag-KTB as a function of the NO_2 concentration in air

Tab. I CH_3I REMOVAL EFFICIENCY OF Ag-KTB IN AIR-NO_2 MIXTURES OF VARIOUS CONCENTRATIONS

Adsorber material: Ag-KTB; $AgNO_3$-impregnation: 86 mg Ag/g KTB (as delivered)

Sweep gas: air, atmospheric pressure, 150°C (dew point 30°C) mixed with NO_2, superficial gas velocity: 25 cm/s

Duration of gas flow: Preconditioning: 24 h
CH_3I-injection: 1 h
Gas flow continued for additional 20 h

Test medium: Mixture of 1.5 ± 0.3 mg $CH_3{}^{127}I$ and 5 - 9 µCi $CH_3{}^{131}I$ per g Ag-KTB (calculated for 10 cm of bed depth)

CH_3I Removal Efficiency in %				
NO_2 (vol. %) in sweep gas	Bed depth in cm			
	2.5	5.0	7.5	10.0
	Stay time in s			
	0.1	0.2	0.3	0.4
1	98.4	99.9981	99.99940	99.99961
2.5	98.5	99.9971	99.99907	99.99936
5.0 +)	98.1	99.986	99.9972	99.9980
10.0 +)	96.7	99.973	99.9954	99.9973
NO_2 (vol. %)	CH_3I Removal Efficiency (%) for each of the 4 successive Ag-KTB Beds			
1	98.4	99.88	68.9	36.2
2.5	98.5	99.81	67.9	31.5
5.0 +)	98.1	99.30	78.2	27.3
10.0 +)	96.7	99.2	83.2	43.4

+) Average of 2 runs

Influence of Granule Size on the Penetration of CH_3I through Ag-KTC

Previous experiments showed that a granule size between 1 and 2 mm for the Ag-KT material will give good removal efficiencies [1]. This granule size can also be handled easily with respect to the adsorber-bed screens. The pressure drop through 10 cm of bed depth at a surface velocity of 25 cm/s is approximately 50 mm of water (for air as sweep gas, atmospheric pressure, room temperature). The granules have almost an ideal ball shape.

Because there were some problems in the reproducibility of the experimental results and a certain degree of separation of different granule sizes within the test beds could not be avoided, penetration tests with test beds from 3 sieve fractions between 1 and 2 mm diameter were performed. The results are given in Fig. 3. For 2.5 and 5.0 cm of bed depth the decrease of penetration with smaller granule size is clearly seen. In the region $< 10^{-2}$ % of penetration, again some irregularties can be observed which we relate to impurities in the CH_3I-sample used. Ag-analysis showed that the Ag-inventory of the different granule fractions increased slightly with decreasing diameter (from 60 mg Ag/g KTB to 64 mg Ag/g KTB), although the different granule fractions were impregnated in one batch.

The test conditions in all experiments, given in Fig. 3, are: Sweep gas at atmospheric pressure and 150°C (dew point 30°C), mixed with 2.5 % NO_2, superficial gas velocity 25 cm/s. Duration of air flow: pre-conditioning: 24 h, CH_3I-injection: 1 h, gas flow continued for additional 19 - 21 h. The loading was approximately 1.5 mg CH_3I/g Ag-KTB, calculated for 10 cm of bed depth.

Influence of the Iodine Loading on the Removal Efficiency of Ag-KTB

Experiments were performed with increasing loadings of CH_3I and I_2 near the saturation of the first of four successive test beds. The experimental results are given in Figs. 4 and 5 and in Tab. II and III. The data represent removal efficiencies integrated over the total loading time and a period of approximately 20 h, in which the sweep gas flow was continued after loading. The experimental conditions are given completely in Tab. II and III.

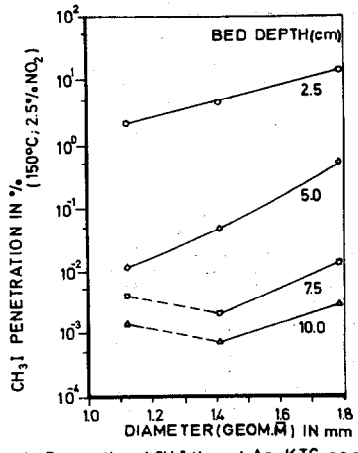

Fig.3 Penetration of CH_3I through Ag-KTC as a function of the granule size

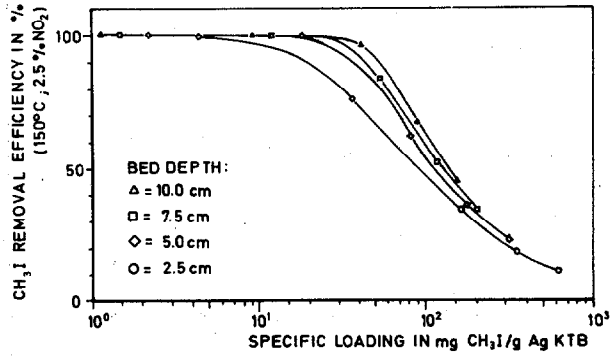

Fig. 4 Removal efficiency of Ag-KTB for CH_3I as a function of the specific loading

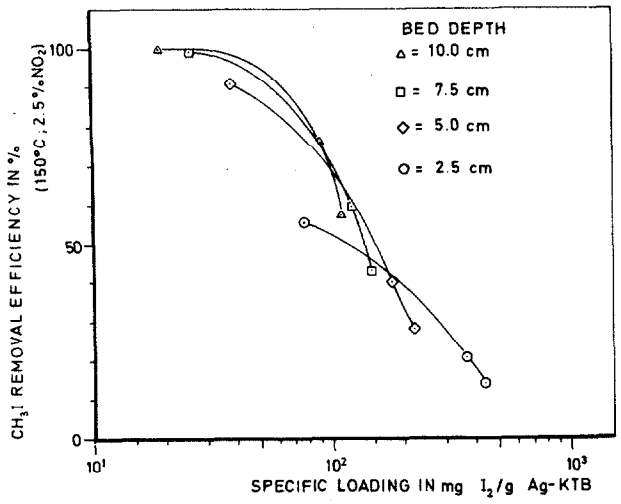

Fig. 5 Removal efficiency of Ag-KTB for I_2 as a function of the specific loading

Tab. II REMOVAL EFFICIENCY OF Ag-KTB FOR CH_3I IN AN AIR-NO_2 MIXTURE AS A FUNCTION OF THE SPECIFIC LOADING

Adsorber material: Ag-KTB; $AgNO_3$-impregnation: 76 mg Ag/g KTB (as delivered)

Sweep gas: air, atmospheric pressure, 150°C (dew point 30°C), mixed with 2.5 % NO_2.

Duration of gas flow: Preconditioning ≥ 24 h
CH_3I-injection: 1 - 2 h
Gas flow continued for additional 20 h

Test medium: Mixture of ≥ 20 µCi $CH_3{}^{131}I$ and $CH_3{}^{127}I$

Test No.	Specific Loading mg CH_3I/g Ag-KTB (calculated for 10 cm of bed depth)	CH_3I Removal Efficiency in %			
		Bed depth in cm			
		2.5	5.0	7.5	10.0
		Stay time in s			
		0.1	0.2	0.3	0.4
1	1.1	99.72	99.9957	99.9976	99.9985
2	9.2	75.7	99.46	99.9923	99.9968
3	41	34.2	63.0	84.0	96.0
4	89	18.4	35.9	52.5	67.6
5	156	11.6	23.0	34.4	45.9
Test No.		CH_3I Removal Efficiency (%) for each of the successive Ag-KTB Beds			
		Bed 1	Bed 2	Bed 3	Bed 4
1		99.7	98.5	44.2	36.0
2		75.7	97.8	98.6	57.9
3		34.2	43.7	56.7	75.3
4		18.4	21.4	25.8	31.8
5		11.6	12.9	14.9	17.6

Tab. III REMOVAL EFFICIENCY OF Ag-KTB FOR I_2 IN AN AIR-NO_2 MIXTURE AS A FUNCTION OF THE SPECIFIC LOADING

Adsorber material: Ag-KTB; $AgNO_3$-impregnation: 63 mg Ag/g KTB (as delivered)

Sweep gas: air, atmospheric pressure, 150°C (dew point 30°C), mixed with 2.5 % NO_2

Duration of gas flow: Preconditioning ≥ 24 h
I_2-injection: main amount in appr. 2 h
Gas flow continued for additional 20 h

Test medium: Mixture of ≥ 6 µCi ^{131}I and $^{127}I_2$

Test No.	Specific Loading mg I_2/g Ag-KTB (calculated for 10 cm bed depth)	I_2 Removal Efficiency in %			
		Bed depth in cm			
		2.5	5.0	7.5	10.0
		Stay time in s			
		0.1	0.2	0.3	0.4
1	20	55.9	91.0	99.83	99.956
2	91	20.9	40.5	59.1	76.0
3	111	14.3	28.8	43.4	57.5
Test No.		I_2 Removal Efficiency (%) for each of the 4 successive Ag-KTB Beds			
		Bed 1	Bed 2	Bed 3	Bed 4
1		55.9	79.5	98.1	73.7
2		20.9	24.7	31.4	41.3
3		14.3	16.8	20.5	24.9

Desorption Behaviour of Iodine from Ag-KT Materials at High Temperatures

The desorption of iodine from Ag-KTB and Ag-KTC was tested at a temperature of 300°C (Fig. 6). The test beds of 10 cm depth were loaded with a mixture of $CH_3{}^{131}I$ and $CH_3{}^{127}I$ and the penetration of ^{131}I was measured by means of downstream charcoal traps cooled to room temperature. In addition to the very low penetration during loading, practically no desorption could be detected over a period up to 33 days of continuous air flow at 300°C. After this period, the experiment was finshed with respect to the decay of the ^{131}I on the test bed. The superficial air velocity was 25 cm/s during these experiments.

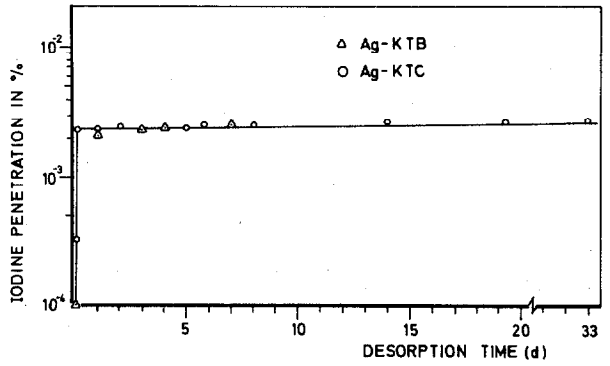

Fig.6 Iodine desorption from different Ag-KT materials at 300°C

Isotopic Exchange with Ag ^{127}I on the Surface of Ag-KTB

Some CH_3I removal experiments at 150°C were performed with Ag-KTB, preloaded with $CH_3{}^{127}I$ so that the $AgNO_3$-impregnation was partly converted into $Ag^{127}I$. The data for the removal efficiencies, given in Tab. IV, were unexpected high. Experiments with Ag-KTB test beds, in which the $AgNO_3$ impregnation was nearly converted in total to $Ag^{127}I$, still furnished considerable removal efficiencies. The unimpregnated KTB-material does not show any removal efficiency under the same conditions, so that the data given in Tab. IV could be discussed as the result of an isotopic exchange reaction of the type:

$$Ag^{127}I + CH_3{}^{131}I \rightleftharpoons Ag^{131}I + CH_3{}^{127}I.$$

In Fig. 7 the penetration of $CH_3{}^{131}I$ through preloaded Ag-KTB test beds (2.5 cm bed depth) is given as a function of silver residue still in the form of $AgNO_3$ (Ag_{sol}). From an extrapolation of the drawing it can be seen that still after complete conversion of the $AgNO_3$ into $Ag^{127}I$ the penetration of the test bed will be only around 30 %. It may be mentioned that the remaining amount of 3.6 mg Ag_{sol}/g KTB could not be converted into $Ag^{127}I$ with $CH_3{}^{127}I$ in considerable excess during the preloading period.

In further experiments one more order of magnitude of ^{131}I was removed by the preloaded Ag-KTB test bed than could be related to the chemical reaction of the test medium of $CH_3{}^{131}I$ and $CH_3{}^{127}I$ with $AgNO_3$. The conclusion can be drawn that at elevated temperature Ag-KT material with an impregnation converted to AgI from off-gas iodine could be reused after radioactive decay of the ^{131}I and so extended service time could be reached. This procedure may be limited by the need for ^{129}I removal.

Experiments to evaluate the isotopic exchange at room temperature showed a reaction rate too low for practical filtering purpose.

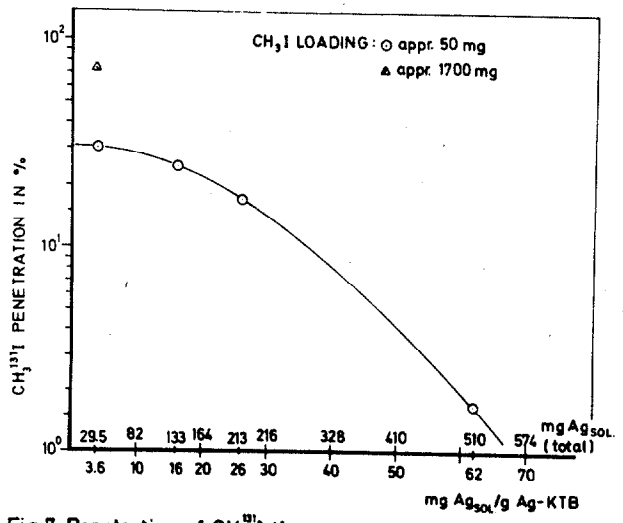

Fig.7 Penetration of $CH_3^{131}I$ through preloaded Ag-KTB as a function of Ag in soluble form

Tab. IV REMOVAL EFFICIENCY OF PRELOADED Ag-KTB FOR ^{131}I (IN THE FORM OF $CH_3{}^{131}I$)

Adsorber material: Ag-KTB; $AgNO_3$-impregnation: 69 mg Ag/g KTB (as delivered)

Sweep gas: air, atmospheric pressure, 150°C (dew point 30°C), mixed with 2.5 % NO_2

Duration of gas flow: same as in Tab. II

Test medium: ≥ 2.4 µCi $CH_3{}^{131}I$/g Ag-KTB, mixed with appr. 1.5 mg $CH_3{}^{127}I$/g Ag-KTB (total loading appr. 50 mg CH_3I per run)

$AgNO_3$ reacted to $Ag^{127}I$ during pre-loading in %	Residual amount of $AgNO_3$ in mg Ag/g Ag-KTB	^{131}I Removal Efficiency in %			
		Bed depth in cm			
		2.5	5.0	7.5	10.0
		Stay time in s			
		0.1	0.2	0.3	0.4
0	62	98.3	99.9949	99.9977	99.9983
58.0	26	82.8	97.8	99.73	99.966
73.9	16	75.1	95.1	99.05	99.88
94.2	3.6	69.5	93.0	98.6	99.71
94.2	3.6 +)	25.9	46.3	60.6	72.4

+) Test medium: 48 mg CH_3I/g Ag KTB (total loading appr. 1700 mg CH_3I for this run).

Effect of Irradiation Exposure of Ag-KTB

Ag-KTB was irradiated with a ^{60}Co source up to $8.6 \cdot 10^8$ rad. It was assumed that radiolytical decomposition of $AgNO_3$ to Ag, Ag_2O and NO_x would seriously reduce the removal efficiency of the material. Some previous removal tests yielded poor results when the $AgNO_3$ impregnation of the Ag-KTC was converted in to Ag and Ag_2O by chemical reaction. The data from the removal efficiency tests with preirr diated Ag-KTB are given in Tab. V. There are some unexpected variations in the removal efficiencies which, obviously, do not depend on irradiation dose, but the overall picture does not show a definite trend. The effect of the irradiation dose seems not to be significant in this region.

Since the Ag-KTB was preconditioned with an air-NO_2 mixture for 24 h before the removal efficiency tests, one could expect that some of the Ag or Ag_2O from radiolytical decomposition will react back to $AgNO_3$. This would result in better removal efficiencies. Therefore, samples of Ag-KTB which were irradiated up to a dose of $8.6 \cdot 10^8$ rad were analyzed for the amount of water soluble impregnation. The data obtained were similar to those of unirradiated Ag-KTB. In addition, no $AgNO_2$ could be detected in the water leach.

Some CH_3I removal experiments were performed with sweep gas without NO_2 (Tab. VI). The data do not show a unique trend depending on the irradiation dose.

From all experimental data it can be concluded that there is no important influence on the removal efficiencies of Ag-KTB from irradiation up to $8.6 \cdot 10^8$ rad.

Tab. V CH_3I REMOVAL EFFICIENCY OF IRRADIATED Ag-KTB IN AN AIR-NO_2 MIXTURE AS A FUNCTION OF ^{60}Co IRRADIATION DOSE

Adsorber material: Ag-KTB; $AgNO_3$-impregnation: 67 mg Ag/g KTB (as delivered)

Sweep gas: air, atmospheric pressure, 150°C (dew point 30°C) mixed with NO_2, superficial gas velocity: 25 cm/s

Duration of gas flow: Preconditioning ≥ 24 h
CH_3I-injection: 1 h
Gas flow continued for additional ≥ 20 h

Test medium: ≥ 2 µCi $CH_3{}^{131}I$/g Ag-KTB, mixed with $CH_3{}^{127}I$

Irradiation before test run in rad	Specific Loading mg CH_3I/g Ag-KTB (calculated for 10 cm bed depth)	CH_3I Removal Efficiency in %			
		Bed depth in cm			
		2.5	5.0	7.5	10.0
		Stay time in s			
		0.1	0.2	0.3	0.4
$1.05 \cdot 10^7$	1.5 ± 0.5	98.6	99.9963	99.99910	99.99948
$1.05 \cdot 10^7$	"	98.5	99.9960	99.9979	99.9990
$1.0 \cdot 10^8$	"	99.75	99.9988	99.99942	99.99965
$1.0 \cdot 10^8$	"	98.0	99.957	99.9983	99.99920
$3.0 \cdot 10^8$	"	95.4	99.945	99.9980	99.9989
$8.6 \cdot 10^8$	"	99.67	99.9931	99.9971	99.9981
$1.05 \cdot 10^7$	47 ± 5	32.7	61.2	82.6	96.1
$3.0 \cdot 10^8$	"	34.0	63.5	84.8	96.6
$8.6 \cdot 10^8$	"	30.7	58.3	81.5	94.8

Tab. VI CH_3I REMOVAL EFFICIENCY OF IRRADIATED Ag-KTB IN WET AIR AS A FUNCTION OF ^{60}Co IRRADIATION DOSE

Adsorber material, impregnation: same as in Tab. V

Sweep gas: air, atmospheric pressure, 30°C, 70 % R.H.

Duration of gas flow, CH_3I-injection: same as in Tab. V

Test medium: 1.5 ± 0.5 mg $CH_3{}^{127}I$ and ≥ 9 µCi $CH_3{}^{131}I$ per g Ag-KTB (calculated for 10 cm bed depth)

Irradiation before test run in rad	CH_3I Removal Efficiency in %			
	Bed depth in cm			
	2.5	5.0	7.5	10.0
	Stay time in s			
	0.1	0.2	0.3	0.4
0	88.1	99.15	99.94	99.9963
$1.05 \cdot 10^7$	87.5	99.23	99.84	99.950
$1.05 \cdot 10^7$	87.8	99.08	99.67	-
$1.0 \cdot 10^8$	86.5	98.0	99.89	99.9926
$1.0 \cdot 10^8$	84.1	99.0	99.93	99.978
$3.0 \cdot 10^8$	82.0	98.1	99.63	-

III. Removal of Iodine from Reprocessing Plant Off-gas

Samples of Ag-KTB were tested in by-passes to the off-gas ducts in a reprocessing plant, using the Purex process. The sample stations were situated behind the washers (water) for the dissolver off-gas and the off-gas from solvent and waste tank. The off-gases are filtered by HEPA-filters before reaching the samplers. Upstream of the Ag-KTB test beds the off-gases are heated to 150°C; at the same temperature, the test beds are operated. Dissolver off-gas and tank off-gas are treated by different samplers of the same type. After various periods of time the test beds were removed and the ^{129}I in the Ag-KTB test beds was measured in the form of ^{130}I after neutron activation. Also chemical analysis was performed for comparison.

In Figs. 8 and 9 the cumulative removal efficiencies as a function of the specific iodine loading are given for three test periods. The total amount of iodine in the off-gas of the dissolver was higher by factors between 10^1 and 10^3, compared with the iodine amount in the tank off-gas. On the basis of equal loading, the Ag-KTB beds showed better performance in the dissolver off-gas than in the tank off-gas. The decontamination

factor reached for test beds up to 7.5 cm are relatively high with respect to the specific iodine loading of the Ag-KTB. The calculated loading for the sum of ^{129}I and ^{127}I is appr. 20 % higher than for ^{129}I alone. In all runs the superficial gas velocity was 25 cm/s and the impregnation 86 mg Ag/g KTB (as delivered).

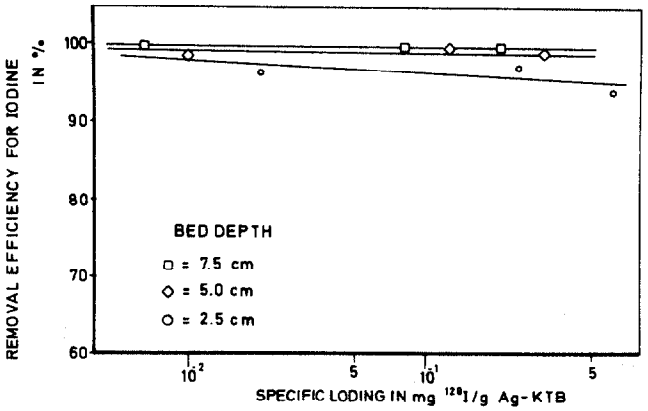

Fig.8 Removal efficiency of Ag-KTB for iodine in the off-gas from solvent and waste tanks as a function of the specific loading

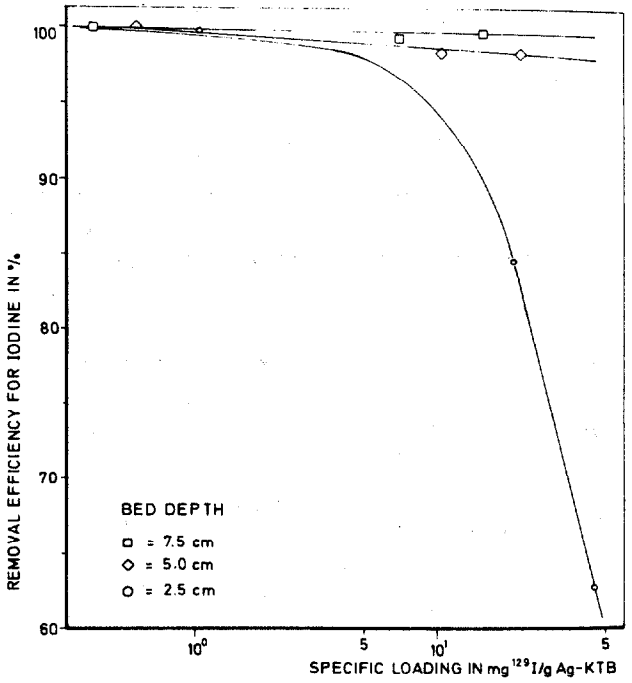

Fig.9 Removal efficiency of Ag-KTB for iodine in the dissolver off-gas as a function of the specific loading

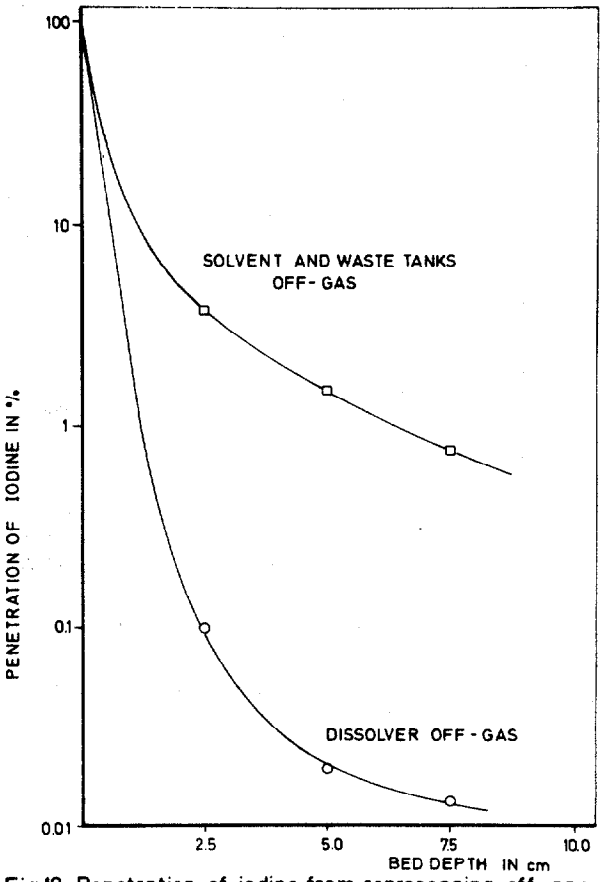

Fig.10 Penetration of iodine from reprocessing off-gas through Ag-KTB as a function of the bed depth

Tab. VII AMOUNT OF ^{129}I IN OFF-GAS SAMPLERS

Run No.	Penetrations given in Fig. No.	^{129}I in sampler (dissolver off-gas) in mg	^{129}I in sampler tank off-gas in mg
I	10	19	0.16
II	11	171	0.32
III	12	373	5.0

In Figs. 10, 11 and 12 the penetration of iodine as a function of the bed depth is given for the three runs reported. The total amount of ^{129}I, trapped in the samplers including one additional "safety trap", is given in Tab. VII.

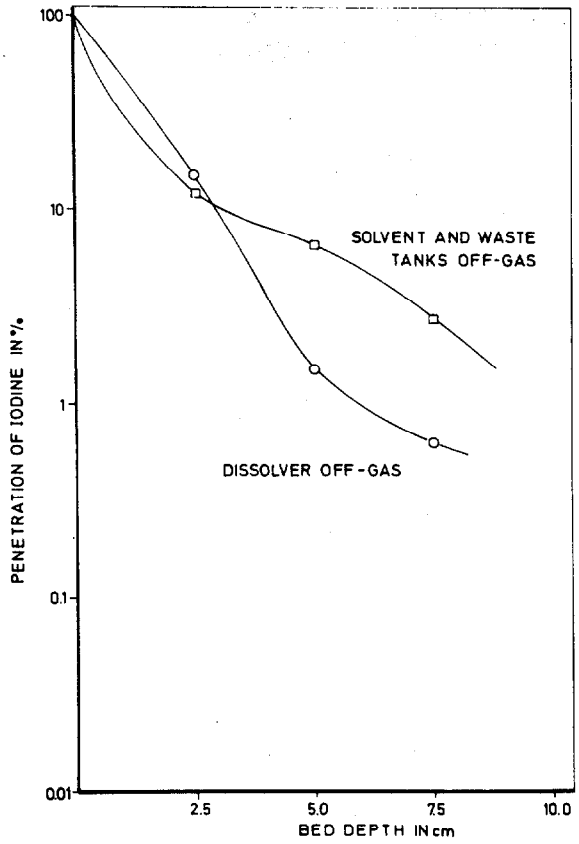

Fig.11 Penetration of iodine from reprocessing off-gas through Ag-KTB as a function of the bed depth

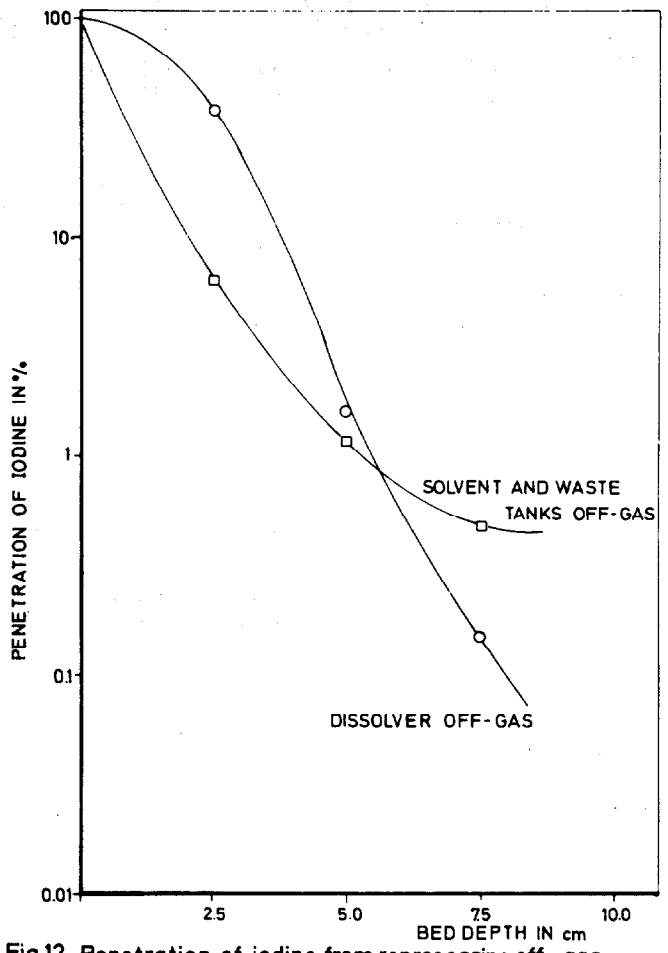

Fig.12 Penetration of iodine from reprocessing off-gas through Ag-KTB as a function of the bed depth

For a proposed full-sized prototype iodine filter, the operating conditions with respect to temperature and superficial gas velocity will be the same as given for the Ag-KTB samplers. At present, we suppose to have a bed depth of approximately 30 cm which will result in a pressure drop of 120 - 200 mm of water. The filter material will counterflow the off-gas and the iodine-saturated Ag-KTB will be removed discontinuously. The price for the Ag-KTB adsorber material is now around 15 $ per kg. Under the given conditions, we expect that per g of iodine to be removed appr. 0.9 g of silver will be needed and a DF > 99.9 % will be reached.

REFERENCES

(1) J.G. WILHELM, Trapping of Fission Product Iodine with Silver-impregnated Molecular Sieves; ACTES DU CONGRES INTERNATIONAL SUR LA DIFFUSION DES PRODUITS DE FISSION, Saclay 4. - 6. Nov. 1969, p. 265-283.

(2) J. G. WILHELM and H. SCHUETTELKOPF, Inorganic Adsorber Materials for Trapping of Fission Product Iodine; PROCEEDINGS of the ELEVENTH AEC AIR CLEANING CONFERENCE, CONF 700816, Dec. 1970, p. 568 - 578.

DISCUSSION

PENCE: Unless I misinterpreted your paper or made an error in my calculations, I conclude that your minimum concentrations in these tests were about 10 to 100 micrograms per cubic meter; is this correct? And, if so, did you conduct any tests in which you looked at lower concentrations?

WILHELM: Which kind of tests do you mean; in the laboratory or in-place tests?

PENCE: In the laboratory.

WILHELM: There was a rather wide range of concentrations covered. I don't know to which experiment you refer at the moment.

PENCE: I was looking for general effects at low concentrations. I would expect this type material to be less effective than others in removing radioiodine at lower concentrations. I am curious about the minimum initial concentrations.

WILHELM: Normally, we had a concentration in these experiments of 3 milligrams per cubic meter. We went higher in the experiments where we checked the capacity of the material. In earlier experiments, reported at the 11th Air Cleaning Conference, we showed results with practically the same material down to a concentration range of at least four orders of magnitude and there was no difference in the removal efficiency.

KOVACH: Have you checked the penetration figures to determine if penetration occurred in one particular downstream path of your beds?

WILHELM: Yes, we did that in experiments reported at the 11th Air Cleaning Conference. We tried that because we assumed that the penetrating component, or whatever else you like to name it, may have been in particulate form. Putting a HEPA filter between the third and fourth test beds didn't alter the removal efficiency of the assembly. Therefore, we could not make sure that this penetrating material is in the form of particles.